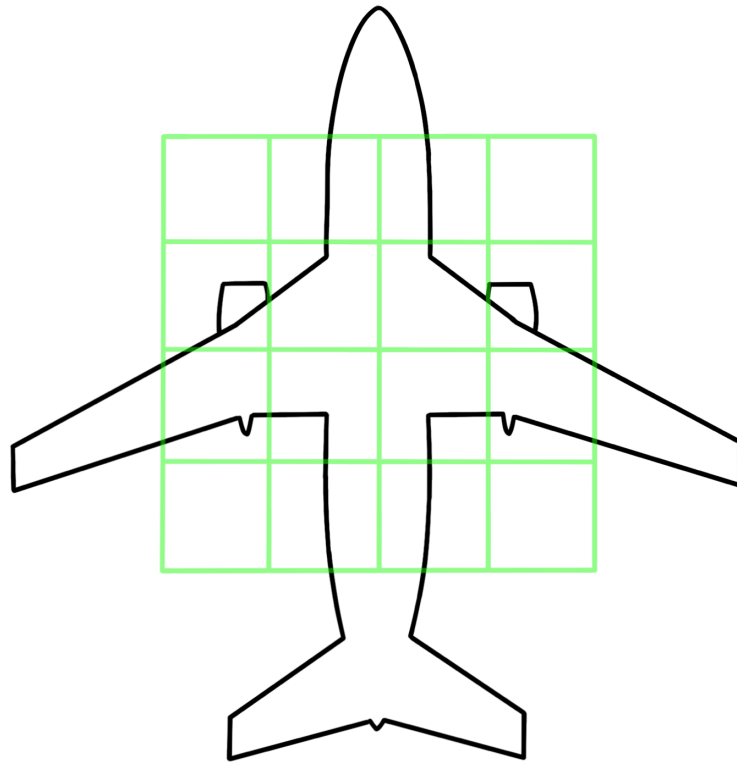




**CHALMERS**  
UNIVERSITY OF TECHNOLOGY



# Overflying measurements using microphone arrays

An investigation of algorithms for sound source localization  
of complex moving objects

Master's thesis in Sound & Vibration

Enes Fehratovic



MASTER'S THESIS 2022

# Overflying measurements using microphone arrays

An investigation of algorithms for sound source localization of  
complex moving objects

ENES FEHRATOVIC



**CHALMERS**  
UNIVERSITY OF TECHNOLOGY

Department of Applied Acoustics  
*Sound & Vibration*  
CHALMERS UNIVERSITY OF TECHNOLOGY  
Gothenburg, Sweden 2022

Overflying measurements using microphone arrays  
An investigation of algorithms for sound source localization of complex moving objects  
ENES FEHRATOVIC

© ENES FEHRATOVIC, 2022.

Supervisor: Dr. Henri Siller, DLR  
Supervisor: Timo Schumacher, DLR  
Examiner: Assoc. Prof. Jens Ahrens, Department of Applied Acoustics

Master's Thesis 2022  
Department of Applied Acoustics  
Sound & Vibration  
Chalmers University of Technology  
SE-412 96 Gothenburg  
Telephone +46 31 772 1000

Cover: Illustration of an aircraft with mesh grid following the trajectory for sound source localization. In reality the mesh grid consists of thousands of grid points.

Typeset in L<sup>A</sup>T<sub>E</sub>X  
Printed by Chalmers Reproservice  
Gothenburg, Sweden 2022

Overflying measurements using microphone arrays

An investigation of algorithms for sound source localization of complex moving objects

ENES FEHRATOVIC

Department of Applied Acoustics

Chalmers University of Technology

## Abstract

It is common to find airports in the vicinity of greater cities where aircraft causes health inflicting noise pollution. Deutsches Zentrum für Luft und Raumfahrt (German Aerospace Center) have been a contributor in reducing sound emissions from aircraft by proposing design changes backed by their research and experiments. To be able to evaluate various design attempts in a real life scenario, sound sources must be localized and quantified in an overflying measurement. At their private airfield they conduct experiments using a microphone phased array. With post processing techniques and the deconvolution algorithm, DAMAS, they have managed to localize and quantify sound sources of aircraft.

DAMAS has been used by the German Aerospace Center since 2006. In recent time they have been eager to investigate more novel algorithms for sound source localization, and one in particular, called CLEAN-T. The goal of this thesis is to investigate how CLEAN-T works and implement it in python code in order to evaluate the results. This would be among the first attempts to use CLEAN-T on overflying measurements at this scale. Both CLEAN-T and DAMAS requires beamforming to be performed in order to enable further deconvolution of the results. The implementation of CLEAN-T was successful and interesting results were obtained. The main advantage of CLEAN-T is that it operates exclusively in the time domain whereas DAMAS is a frequency domain algorithm. This means that CLEAN-T can take the movement of the object into account whereas frequency domain algorithms are better suited for stationary sources. Although CLEAN-T can cause a masking effect leading to undetected sources who are very close to each other, CLEAN-T can operate in lower frequencies than DAMAS. It also scales better for greater amount of focus points in the grid, meaning that for higher resolution or larger area of analysis, CLEAN-T is faster.

Keywords: sound source localization, aircraft, beamforming, deconvolution, microphone array



## Acknowledgements

I would like to express my great appreciation to Dr. Henri Siller and Timo Schumacher for their patient guidance, enthusiastic encouragement and useful critiques of this research work. I would also like to thank the German Aerospace Center (DLR) for providing me with data of overflying measurements. My grateful thanks are also extended to the staff of DLR for enabling me to visit their facilities and allowing me to observe their daily operations. I would like to offer my special thanks to Assoc. Prof. Jens Ahrens for their support and guidance.

Finally I would like to thank my parents and partner for their support and encouragement throughout my studies.

Enes Fehratovic, Gothenburg/Berlin, June 2022



# List of Acronyms

Below is the list of acronyms that have been used throughout this thesis listed in alphabetical order:

BF	Beamforming
BPF	Blade Passing Frequency
CLEANT	CLEAN Algorithm in Time Domain
CLEAN-SC	CLEAN Algorithm for Coherent Sources
CSM	Cross Spectral Matrix
DAMAS	Deconvolution and Mapping of Acoustic Sources (Algorithm)
dB	Decibel
DFT	Discrete Fourier Transform
DLR	Deutsches Zentrum für Luft und Raumfahrt (German Aerospace Center)
DOA	Degree Of Arrival
FFT	Fast Fourier Transform
GPS	Global Positioning System
PSF	Point Spread Function
SPL	Sound Pressure Level
TOB	Third Octave Band
ULA	Uniform Line Array



# Contents

<b>List of Acronyms</b>	<b>ix</b>
<b>1 Introduction</b>	<b>2</b>
1.1 Background . . . . .	2
1.2 Setup . . . . .	3
<b>2 Theory</b>	<b>5</b>
2.1 Wave propagation . . . . .	5
2.2 Discrete Fourier Transform . . . . .	6
2.3 Auto & Cross Spectrum . . . . .	7
2.4 Doppler Effect . . . . .	7
2.5 Microphone Phased Array . . . . .	9
<b>3 Methods</b>	<b>13</b>
3.1 Beamforming . . . . .	13
3.1.1 Time-Domain-Formulation . . . . .	14
3.1.2 Frequency-Domain-Formulation . . . . .	15
3.2 DAMAS . . . . .	16
3.3 CLEAN . . . . .	17
3.4 CLEAN-SC . . . . .	19
3.5 CLEAN-T . . . . .	20
3.6 Implementation . . . . .	22
<b>4 Results</b>	<b>24</b>
4.1 Simulated overflying measurements of a single sound source . . . . .	25
4.1.1 Diagonal removal deactivated . . . . .	26
4.1.2 Diagonal removal activated . . . . .	28
4.2 Simulated overflying measurements of two sound source . . . . .	29
4.2.1 Diagonal removal deactivated . . . . .	30
4.2.2 Diagonal removal activated . . . . .	32
4.2.3 Diagonal removal activated and low loop gain . . . . .	33
4.2.4 Diagonal removal activated and single 1000 Hz TOB detection . . . . .	35
4.3 Recorded overflying measurements from 2016 . . . . .	37
4.3.1 Diagonal removal deactivated . . . . .	37
4.3.2 Diagonal removal activated . . . . .	39
4.4 Recorded overflying measurements from 2019 . . . . .	40
4.4.1 Diagonal removal deactivated . . . . .	41

4.4.2	Diagonal removal activated . . . . .	43
4.4.3	Diagonal removal activated and low loop gain . . . . .	44
4.4.4	Diagonal removal activated and single 1000 Hz TOB detection	46
4.4.5	DAMAS vs. CLEAN . . . . .	48
<b>5</b>	<b>Analysis</b>	<b>50</b>
<b>6</b>	<b>Conclusion</b>	<b>52</b>
	<b>Bibliography</b>	<b>54</b>

# 1

## Introduction

This section will introduce the reader to this study and why it was performed. The reader will understand the problem formulation, why it is important to be able to localize and quantify sound sources of overflying aircraft and the necessary tools to acquire such information.

### 1.1 Background

It is fairly common to find an airport in the vicinity of a greater city. Living in a urban area, an airport is usually no more than 30 minutes away. This means that the traffic to and from the airport often passes over nearby towns, suburb areas or parts of the inner city. With their jet engines and high speed the aircraft causes a lot of noise, noise that is polluting the environment wherever it passes. This can cause great disturbance to a lot of people, especially during uncomfortable hours. Long term impacts of such noise can be quite devastating and lead to anxiety, depression and cardiovascular diseases. In a big study performed by WHO, researchers could link all the above mentioned conditions to noise pollution which also raised the awareness of the drastic health impacts caused by noisy environments [12]. In order to maintain the convenience of having airports close to cities and building sustainable urban environments great effort is made in order to keep the noise levels down. Common people who are affected by the noise pollution are not the only beneficiary group. Health benefits, achieved through lower sound emitted by aircraft, is the main reason why these studies are performed. But aircraft manufacturers are paying significant noise taxes which is based on the noise levels when landing and these taxes can vary at different airports [9]. In order to be able to target the main noise contributors on an aircraft the noise must first be located with high precision and correct levels. Thus attempts, in order to lower the emitted noise levels, can be properly evaluated. German Aerospace Center (DLR) have made contributions in this field by performing overflying measurements. Through complex post processing methods such as beamforming and a deconvolution algorithm called DAMAS they have successfully been able to localize and quantify sounds sources of aircraft. The DAMAS algorithm was developed by NASA in 2004 [3] and was further studied and implemented by DLR in the following years [7]. In the years passed since, extensive research has been made in the field of sound source localization and further development on already existing algorithms. For that reason DLR wants to investigate if there are new approaches that could surpass or complement the DAMAS algorithm. One of the most promising algorithm which is on the agenda of DLR is the

CLEANT algorithm. It is based on the traditional CLEAN algorithm but exclusively performed in time domain, hence the added letter "T" for time domain. A time domain algorithm could possibly reduce the short comings of algorithms solely performed in the frequency domain, which are generally not suitable for moving sound sources.

## 1.2 Setup

Measurements are performed at DLR:s private airfield Magdeburg-Cochstedt, 190 km from Berlin city. DLR has their own research aircraft called ATRA which is initially an Airbus A320-232 with V2500 long cowl engines and can be seen in figure 1.1.



**Figure 1.1:** The research aircraft of DLR flying above the microphone array

On the ground there is a microphone phased array with a total of 238 electret microphones. The size of the array is 35x40 m and the shape is a multi-arm logarithmic spiral stretched in the direction of flight which can be seen in figure 1.2 and 1.3.



**Figure 1.2:** The microphone array located at the Magdeburg-Cochstedt private airfield

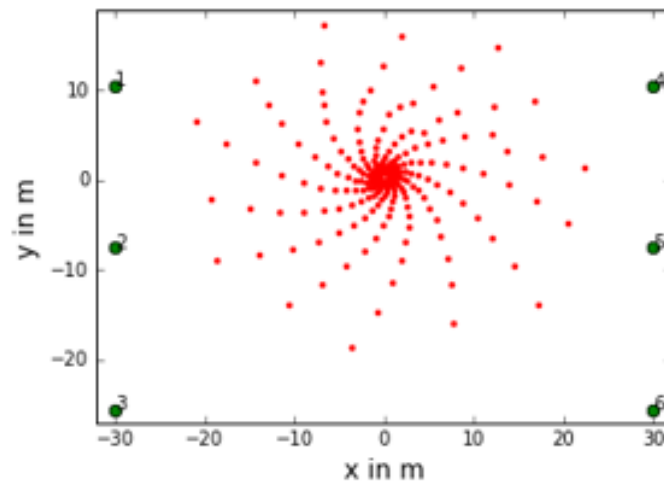


**Figure 1.3:** An illustration of the microphone array where size and shape is better observed.

In May 2016 baseline experiments were performed at the private airfield and in September 2018 and July 2019 noise modified experiments were performed. In this study measurements from 2016 and 2019 are mainly used.

Information and figures of the private airfield, microphone array and experimental aircraft was provided by DLR.

# 2

## Theory

In the following sections I will cover the theoretic knowledge necessary to understand the purpose of the algorithms and their functionality which will be covered in later stages of the thesis. A point source refers to a single derivative of a sound source.

### 2.1 Wave propagation

Sound can be explained as pressure fluctuations which travels through a medium such as air or fluids. The motion of sound waves through air in one dimension can be described by the classic formula in equation 2.1, also known as the wave equation.

$$\frac{\partial^2 p}{\partial x^2} - \frac{1}{c_0^2} \frac{\partial^2 p}{\partial t^2} = 0 \quad (2.1)$$

Where  $p$  is pressure,  $x$  is a measure of distance,  $t$  is time and  $c_0$  is the speed of sound. The wave equation is a partial differential equation that combined several equations in order to describe the propagation of waves. These equations can be observed in equations 2.2 - 2.4.

Equation of continuity:

$$\frac{\partial p}{\partial t} + \rho_0 \frac{\partial u}{\partial x} = 0 \quad (2.2)$$

Where  $\rho$  is the density of the medium, in this case air and  $u$  is the velocity. Equation of motion:

$$\rho_0 \frac{\partial u}{\partial x} + \frac{\partial p}{\partial x} = 0 \quad (2.3)$$

Gas equation:

$$\frac{\partial p}{\partial \rho} = \frac{kRT}{m} \quad (2.4)$$

Where  $k$  is the ratio of specific heat,  $R$  is the gas constant,  $T$  is temperature in Kelvin and  $m$  is mass. A general solution to the wave equation in one dimension is:

$$p(x, t) = f\left(t \pm \frac{x}{c_0}\right) \quad (2.5)$$

for plane waves where the pressure is dependent on a function of time  $t$  and distance  $x$ . The solution for a two dimensional plane wave propagating in a third dimension is obtained by the real part of

$$p(x, t) = p(x)e^{j(\omega t)} \quad (2.6)$$

To understand the difference between a plane wave and a spherical wave in this context, assume a sound source oscillating with a certain frequency. The sound source can be a point source that radiates sound in all directions. At lower frequencies a longer wavelength is generated by the point source. If a receiving point is placed at a certain distance to the source the receiving point is more prone to experience the curvature of the radiated sound, thus experiencing spherical waves. At higher frequencies the wavelength is much shorter and the curvature of the source is therefore not as significant for the same receiving point. If the receiving point is placed at a greater distance from the source it is more likely to achieve plane waves as a uniform sound-front even for lower frequencies. Therefore, at a receiving position close to the source, relative to the frequency wavelength, we can assume spherical waves. If the receiving point is far relative to the frequency wavelength, we can assume plane waves. The wave equation can be transformed to account for spherical coordinates

$$\frac{\partial^2 p}{\partial r^2} + \frac{2\partial p}{r\partial r} - \frac{1}{c_0^2} \frac{\partial^2 p}{\partial t^2} = 0 \quad (2.7)$$

where  $r$  is the radius of the spherical sound wave. A general solution to the wave equation with spherical coordinates is given by

$$p(r, t) = \frac{1}{r} f\left(t \pm \frac{r}{c_0}\right) \quad (2.8)$$

where the incoming wave ( $t + \frac{r}{c_0}$ ) is often neglected and an equation for outwards propagating harmonic wave can be formulated:

$$p(r, t) = \frac{A}{r} e^{j(\omega t - kr)} \quad (2.9)$$

where  $A$  is the amplitude of the sound source,  $\omega$  is the angular frequency and  $k$  is the wave number.

## 2.2 Discrete Fourier Transform

Without contradictions, it is safe to say that Discrete Fourier Transform (DFT) is one of the most powerful assets in digital signal processing. DFT is an algorithm that transforms a signal from time domain into frequency domain. This is of course extremely valuable for analysis purposes and further manipulation of a signal. The Fast Fourier Transform (FFT) is essentially a calculation algorithm to solve DFT calculations more efficiently and reduce the computation time, which is especially useful when handling large amounts of data. DFT is a calculation of order  $\mathcal{O}(n^2)$  and FFT is a calculation of order  $\mathcal{O}(n \log n)$  where  $n$  represents discrete points of a finite signal. For the FFT to operate under optimal conditions the block size of data should be in order of  $2^n$ . The reason for this is to enable the FFT algorithm to continuously divide the operation into smaller chunks and avoid redundant calculations by doing so.

Performing a DFT yields information such as frequency spectrum, amplitude and phase from a signal. Due to the simple reason that a digital computer cannot handle

a continuous-time signals, the signal needs to be sampled in order to be studied. The number of samples ( $N$ ) can vary depending on the signal content. A rule of thumb is that the signal should be sampled with a frequency  $f_s$ , where  $f_s$  is at least twice as high as the highest frequency of the signal. This is also known as the Nyquist frequency. If this criteria is not met the signal can not be accurately displayed and valuable information will be lost in the process of sampling. A much higher sampling rate would of course generate more detailed data. The mathematical formula for the DFT is

$$X(k) = \sum_{n=0}^{N-1} x(n) \cdot e^{-j\frac{2\pi kn}{N}} \quad (2.10)$$

where  $k$  is the Fourier coefficient,  $n$  is the sample number and  $N$  is the total amount of samples. The DFT assumes that the signal is periodic, therefore the transformed spectrum is periodic and double-sided. The transformed signal is not scaled. This means that in order to get an accurate amplitude of the signal, scaling should be applied as following.

$$\bar{X}(k) = \frac{1}{N} \cdot X(k) \quad (2.11)$$

## 2.3 Auto & Cross Spectrum

Auto-spectrum is a useful processing step because it discards the imaginary part of the signal through complex conjugate multiplication. This generates a squared amplitude, which implies that the auto-spectrum is a measure of the energy/power of a frequency component. Auto-spectrum is calculated by using the following equation

$$S_{xx}(f_n) = X(f_n) \cdot X(f_n)^* \quad (2.12)$$

where  $X(f_n)$  is the transformed signal and  $X(f_n)^*$  is its complex conjugate. The difference between auto-spectrum and cross-spectrum is that autospectrum uses the same input signal only conjugated where cross-spectrum uses two different input signals. Cross-spectrum can be useful when using multiple measurements in order to reduce the uncorrelated noise in both signals. By squaring the signal, phase information is lost and a fixed phase relation is obtained. This way, the averaging process of the cross-spectrum reduces noise because the average of uncorrelated noise is suppressed. The cross-spectrum between the two signals can be calculated by equation

$$S_{yx}(f_n) = Y(f_n) \cdot X(f_n)^* \quad (2.13)$$

where  $Y(f_n)$  and  $X(f_n)^*$  represent two different signals after performing FFT.

## 2.4 Doppler Effect

Most people have encountered the doppler effect in their everyday life. A typical scenario where this effect is most noticeable is when an ambulance or police vehicle

passes by with their sirens turned on. There is a noticeable shift in frequency when the vehicle approaches and once it passes. This happens because the wavelength of the source sound is smaller in the direction the vehicle moves. Because the sound source is omnidirectional, the sound source and the sound are moving in the same direction. The velocity of the sound source can be subtracted from the speed of sound and vice versa. When the source is leaving the receiver position the velocities of the source and the sound can be added because they move in opposite directions. This causes a longer wavelength as the source is leaving and a shorter wavelength as the source is approaching which can be seen as  $\lambda_1$  and  $\lambda_2$  in figure 2.1. Assume an omnidirectional point source emitting a 1000 Hz pure tone that is moving to the right as in figure 2.1. If a receiver is placed to the right of the source so that the source is approaching the receiver with a constant speed of 30 m/s, the perceived frequency will be different to the one that the source is actually emitting. The change in pitch can be calculated by equation

$$f_{approach} = f \frac{c_0}{c_0 - v} \quad (2.14)$$

where  $f_{approach}$  is the perceived frequency as the source is approaching,  $f$  is the frequency emitted by the source,  $c_0$  is the speed of sound and  $v$  is the constant velocity of the source. For a scenario where the sound source is leaving the equation is similar, the only difference is that the velocities are added instead.

$$f_{leaving} = f \frac{c_0}{c_0 + v} \quad (2.15)$$

With these equations both approaching and leaving frequencies can be calculated which yields  $f_{approaching} = 1096.77$  Hz and  $f_{leaving} = 918.92$  Hz when the sound source is moving to the right at a velocity of 30 m/s assuming that the speed of sound  $c_0 = 340$  m/s.

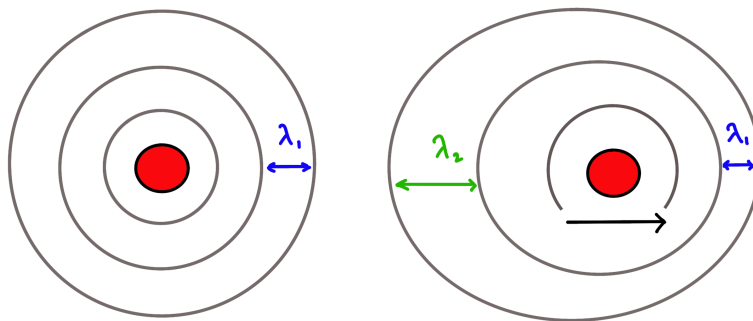


**Figure 2.1:** (Left): Omnidirectional point source. (Right): Omnidirectional point source moving to the right demonstrating the doppler effect.

For overflying measurements using a microphone array the doppler factor is calculated slightly different. The microphone array is located on ground level while the aircraft is passing above it. The frequency which will be received by the microphone array is dependent of the emitted frequency by the aircraft and adhere to

$$f_m = f_e D_f \quad (2.16)$$

where  $f_m$  is the frequency at the microphone location,  $f_e$  is the frequency emitted by the aircraft and  $D_f$  is the doppler factor. Doppler factor in this case depends on the mach number and the emissions angle. Mach number is easily calculated with  $M = v/c_0$ , where  $v$  is the speed of the object, in this case an aircraft, and  $c_0$  is the speed of sound. Emission angle between the aircraft and the microphone array is calculated using simple trigonometry. The doppler factor is the obtained using

$$D_f = \frac{1}{1 - M \cos \theta_e} \quad (2.17)$$

where  $\theta_e$  is the emission angle between the aircraft trajectory and the microphone array as in figure 2.2. Frequency at microphone location is then given by equation 2.16.

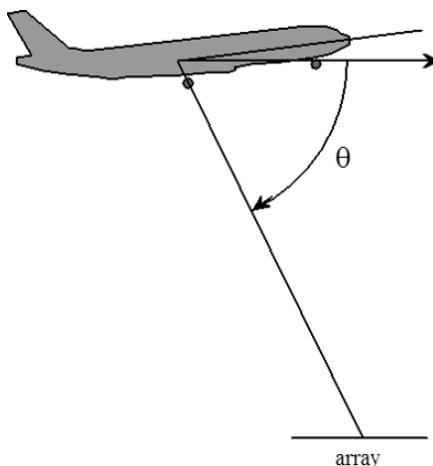


**Figure 2.2:** Illustration of the emission angle.

## 2.5 Microphone Phased Array

Assume an acoustic source emitting sound under free field conditions at a certain position. Beamforming results of that source will not present a perfectly located source. Beamforming result will present the original source surrounded by additional sources spread around the original source that might not really be there. The finite number of microphones in a microphone phased array causes a spatial undersampling. The system response caused by the spatial undersampling is called the point spread function (PSF). The phased array mainly consists of empty space which is resulting in spatial aliasing. In an optimal scenario there would be no space in between the sensors although such devices does not yet exist. There are several factors that affect the PSF in a microphone array, the spacing between the microphones, the amount of microphone sensors and the shape of the microphone array.

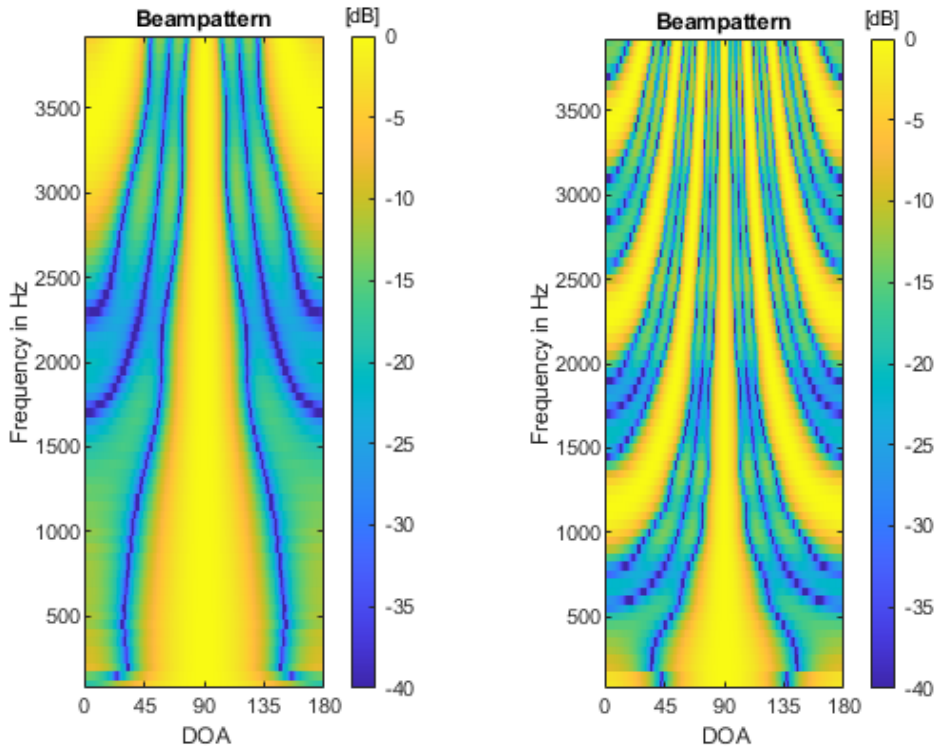


**Figure 2.3:** (Left): Four microphones with an element spacing of 0.1m. (Right): Four microphones with an element spacing of 0.3m.

For demonstration purposes a simple Uniform Line Array (ULA) has been chosen to demonstrate the effects of element spacing and element amount in figure 2.3. The color bar shows that the yellow color represents a sensitivity in certain Degree of Arrival (DOA) along the x-axis. Along the y-axis one can observe how the beam-pattern changes over frequency with a frequency range of 0 – 4000 Hz. It is clearly visible that increasing the distance between the microphone elements has a great impact on the beam-pattern of the array. The space determines at which frequency sidelobes are introduced by using the simple equation

$$f = c_0/\lambda \quad (2.18)$$

where  $f$  is the frequency,  $c_0$  is the speed of sound and  $\lambda$  is the wavelength. In this case the distance between the elements is used as the wavelength in the equation. In the left figure the spacing is 0.1 m which corresponds to the wavelength of a 3400 Hz signal, assuming the speed of sound is 340 m/s. In the figure to the right the spacing is 0.3 m and following by using the 2.18 again the sidelobes of this setup will appear at approximately 1133 Hz. In the right figure several sidelobes can be detected above 1133 Hz which corresponds to,  $n \cdot f$ , where  $f$  is the fundamental frequency corresponding to the distance between microphones. In both figures it can be determined that for very low frequencies the directional of the beam is very wide and therefore rather inaccurate for lower frequencies. Generally the beam width is wider for the array with shorter spacing which can also be observed in figure 2.3

comparing the two figures, the beamwidth of the right configuration is more narrow in the range of 500 – 4000 Hz. This phenomenon can also be observed in figure 2.4.

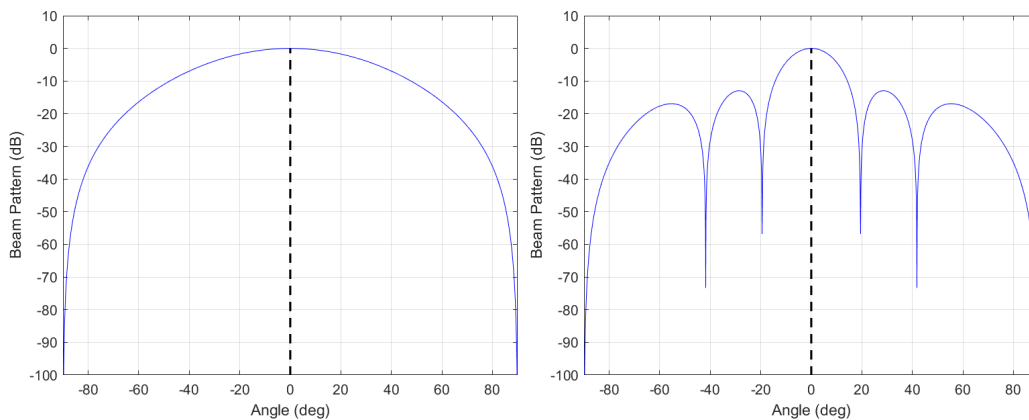


**Figure 2.4:** (Left): Ten microphones with an element spacing of 0.1m. (Right): Ten microphones with an element spacing of 0.3m.

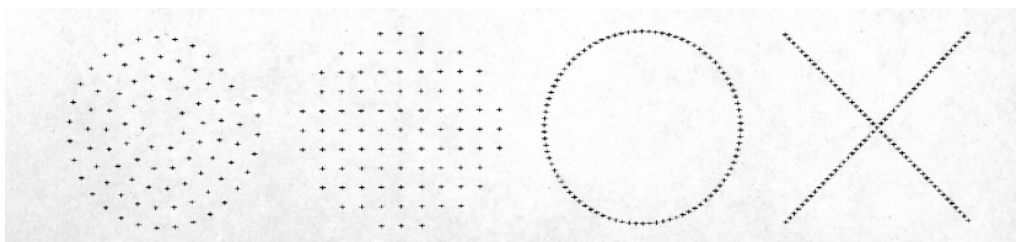


**Figure 2.5:** Four different microphone array configurations. From left: spiral, grid, circle and X-shape. Image source: [2]

Microphone arrays can take many sizes and shapes and there has been extensive research made in pursuit of finding an optimal array design. In 2000 the national German railway company, Deutsche Bahn, initiated a study on optimum array microphone configuration in order to better quantify the noise generated by trains [2]. Four 2D array configurations were tested in a simulated environment, spiral, grid, circle and X shaped arrays which can be seen in figure 2.5. The microphone array for all configurations had a diameter of 4 m, element spacing of 0.4 m for spiral and grid configuration and 0.1 m spacing for circle and X configuration. The source is simulated train noise located at 7.5 m from the microphone array where the train has a velocity of 50 m/s. Source strength detected by the array can be estimated by

$$s_j(t) = \frac{\sum_{m=1}^N p_m(t + r_{jm}(t)/c_0)}{\sum_{m=1}^N r_{jm}^{-1}(t)} \quad (2.19)$$

where  $s_j(t)$  is a source,  $N$  is the total amount of microphones,  $r_{jm}$  is the distance between the source  $s_j$  and the receiving microphone  $p_m$  at time  $t$  and  $c_0$  is the speed of sound. Doppler effect has been neglected in this case and rectangular amplitude weighting window is assumed [2]. All microphone arrays configurations consists

of 90 microphones where the spiral configuration is irregularly spaced and the grid configuration is regularly spaced. The results in 2.6 reveal that the spiral formation generates the most accurate results across the varying frequency bands. Irregular element spacing contributes to lower sidelobes and grating lobes which visibly occurs in the regularly shaped grid configuration in column 2. Grating lobes causes fake sources to appear around the two original sources with equal strength. Circle and X shaped arrays causes significantly different result due to their characteristic shapes which visibly perform worse in all frequency ranges compared to the irregularly shaped spiral.

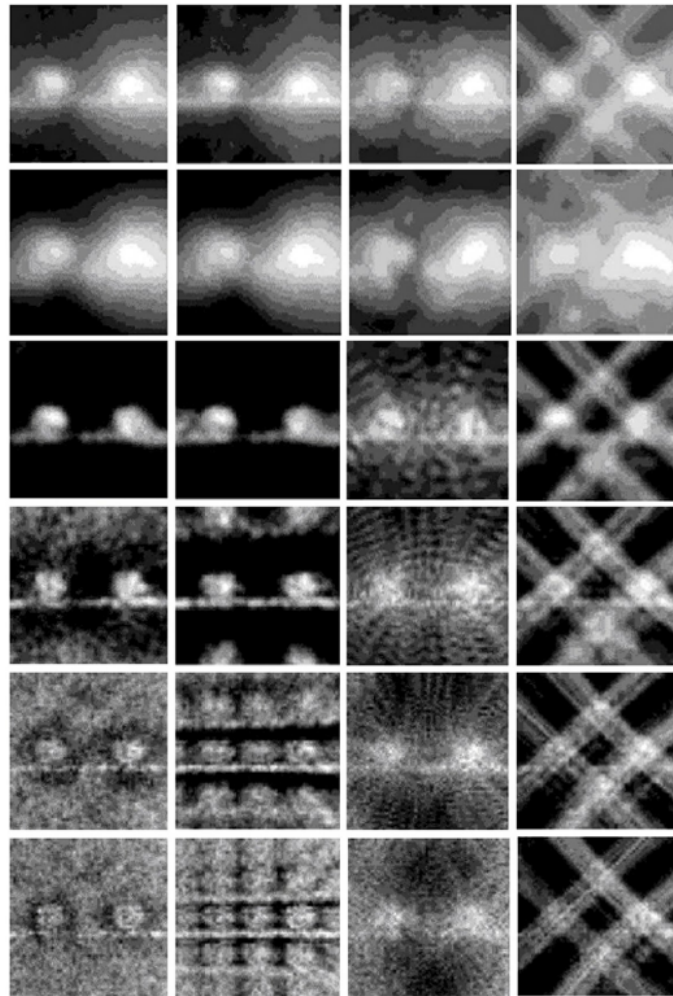


**Figure 2.6:** Column 1: Spiral, Column 2: Grid, Column 3: Circle, Column 4: X-Shape. Row 1: Total levels, Row 2: 200 – 600 Hz, Row 3: 1 – 1.4 kHz, Row 4: 1.8 – 2.2 kHz, Row 5: 3 – 3.4 kHz, Row 6: 3.8 – 4.3 kHz. Image source: [2]

# 3

## Methods

In this section acoustic imaging algorithms are explained. Some algorithms rely heavily on the deconvolution process by suppressing the PSF of the sound sources. Both DAMAS and CLEAN-T aim to improve the results generated by beamforming which is why beamforming is essential in most acoustic imaging approaches. Algorithms that aim to improve the results of beamforming are also extensively increasing the computation cost by evaluating a scanning each single grid which contains points with potential sound sources.

### 3.1 Beamforming

A phased microphone array, also called microphone antenna, refers to a setup of multiple transducers (in this report mainly microphones), first saw the light of day in 1974 and was developed by John Billingsley. Before that beamforming was first incorporated in radar antennas during world war 2 [4]. Today phased arrays are also used in medical imaging using ultrasound. Improvements in data acquisition, computing hardware and software enabled the use of bigger arrays, incorporating more microphones with high sample rates. This massively improved the quantification and localization of sources of complex objects. It is often used for aerodynamic sources in wind tunnels as well as localizing and quantifying moving sources on flying aircraft, trains, motorized vehicles in motion and operating rotors such as turbo engines and helicopters [4]. To successfully localize moving sound sources, the movement of the object must be well known to be able to take it into account.

Howell et al. first demonstrated the possibilities of performing beamforming on aircraft in 1986 [4]. They used a line array consisting of four microphones with a spacing of 3.802 m in between. The microphone array was aligned with the trajectory of the aircraft for the first measurement. This measurement revealed the blade passing frequency of the wing engines. Another measurement was performed this time in transversal alignment of the trajectory. This measurement revealed the location of the wing engines. Later on microphone arrays took different shapes, one that has been proved more efficient is the logarithmic spiral. As mentioned earlier, the movement of the aircraft must be well known which is why nowadays there is a data acquisition for the position relative to the microphone array over time as well as environmental conditions. In order to acquire precise source localization and determine the speed of sound, the environmental conditions are necessary. The speed of sound in air can be approximated by

$$c = 331.4m/s + T \cdot 0.6 m/s , \quad (3.1)$$

where  $c$  is the speed of sound and  $T$  is the temperature in Celsius.

Essentially, beamforming is a technique for processing data acquired from a microphone array in order to achieve an image of located sources in a so called source map. A mesh-grid covering the entire aircraft and following the trajectory of the aircraft contains much smaller grids, so called focus points [3]. Beamforming is repeated for each focus point in this mesh-grid where there is a potential source. For focus points where there so happens to be a source the source is preserved and for focus point not containing a source the source is suppressed. Thus the source map of the aircraft can be generated by repetitively performing beamforming for each focus point [6]. A technique often associated with beamforming is the delay-and-sum approach. In simple words, each source will be recorded by each microphone at different times due to the varying distances. Due to the fact that setup details and environmental parameters are known during the measurements it is fairly straight forward to determine the delay between the signals. The signals are shifted so that they are aligned correctly, summed and then normalized depending on how many signals are available. Delay-and-sum beamforming can be performed in both frequency domain and time domain. When done in the frequency domain, the time delay corresponds to a varying phase shift of the signals. Only beamforming in the time domain allows for non-stationary focus points however.

### 3.1.1 Time-Domain-Formulation

In figure 3.1 a simple setup of delay and sum beamforming can be observed. In this setup there is a known source,  $x$ . Assume that the speed of sound and the various distances between the sound source and the three microphones are known.

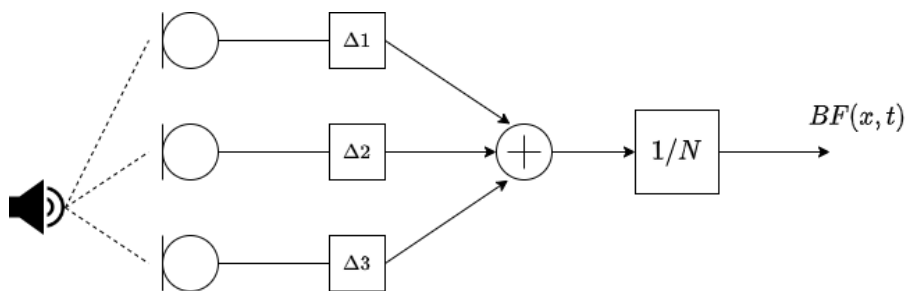


**Figure 3.1:** Illustration of delay and sum beamforming

It is now possible to calculate the delay which should be applied to each microphone signal in order to align the received signals in time, creating an acoustic beam for this particular sound source. The aligned signals are summarized, normalized by the total amount of microphones and the levels at this source location can be determined. In this setup there is only one sound source present and the position is known, that is not the case with overflying measurements with arbitrary sound sources at unknown positions. In overflying measurements the sound sources are

traveling along with the aircraft, the trajectory of the aircraft relative to the microphone array position, is therefore monitored by a GSP and recorded by the data acquisition system so that beamforming can adapt to the moving sources. The grid, covering and following the trajectory of the aircraft, enables calculations of each focus point at each discrete time instance.

The process for time domain beamforming is given by equation

$$b(t, x_j, \{p_m\}) = \frac{1}{K_j(t)} \sum_{m=1}^N w_m \frac{p_m(t + \frac{r_{jm}(t)}{c})}{r_{jm}(t)(1 - M \cos \theta_{jm}(t))^2}, \quad (3.2)$$

$$K_j(t) = \sum_{m=1}^N \frac{w_m}{[r_{jm}(t)(1 - M \cos \theta_{jm}(t))^2]^2} \quad (3.3)$$

where  $p_m$  is the microphone signal between the sound source  $j$  and microphones  $m$ ,  $K_j$  is a normalization factor,  $x_j$  represents the focus points in the grid,  $M$  is the mach number,  $\theta$  the incidence angle of the focus point,  $w_m$  is the spatial weighting coefficient for microphone  $m$  and  $r_{jm}$  the distance between the focus point and microphone [8]. These are parameters of moving sound sources which changes location over time and thus time dependent. This also enables the removal of geometric attenuation from the signal resulting in the sound source levels for a specific focus point [10]. Once this is done for all focus points at all discrete time instances a beamforming source map is obtained.

### 3.1.2 Frequency-Domain-Formulation

Another way to do beamforming is through calculating the CSM which is technique that works in the frequency domain and is well suited for stationary incoherent broadband sources. In a discrete mesh grid covering the aircraft there are many smaller grid points. Assuming there is a sound source in the grid point  $\xi_j$ , the signal at microphone location is then  $s_j \vec{g}_j$ , where  $s_j$  is the complex amplitude of the source and  $\vec{g}_j$  is a  $N$  component complex vector known as the steering vector. Steering vector has the same amount of components as there are microphones and the steering vector models the pressure amplitude at microphone location [11]. In free field the steering vector is given by the Green's function of the Helmholtz equation

$$g_m = \frac{\exp(-2\pi i f \|\vec{x}_m - \vec{\xi}_j\|/c)}{4\pi \|\vec{x}_m - \vec{\xi}_j\|}, \quad (3.4)$$

where  $\|\cdot\|$  is the euclidean norm,  $i$  is the imaginary unit and  $\vec{x}_n = (\mathbf{x}_n, \mathbf{y}_n, \mathbf{z}_n)^T \in \mathbb{R}^3$  are the positions of  $N$  microphones. The autopower,  $A$ , of the source located at  $\xi_j$  can now be estimated by mathematically diminishing the difference between the estimation and the actual pressure vector recorder by the microphones. Since it is a mathematical estimation the constant can be neglected.

$$A(\xi_j) = \frac{1}{2} \frac{g_j^* \langle pp^* \rangle g_j}{\|g_j\|^4} = w_j^* C w_j \quad (3.5)$$

Where  $\langle \cdot \rangle$  is the time average and  $w_j$  is the weighted steering vector and  $C$  is the CSM of the pressure measured by the microphones in frequency domain by using FFT.

$$w_j = \frac{g_j}{\|g_j\|^2} \quad (3.6)$$

$$C = \langle pp^* \rangle \quad (3.7)$$

$C$  is a positive definite matrix because of the definition mentioned in 3.7. This can although lead to exaggerated levels when noise is present. Because of the averaging operation, noise, which is incoherent between microphones, only remains in the autopower. The auto-spectrum makes up the diagonal of the CSM.

$$C = \begin{bmatrix} C_{11} & C_{12} & \dots & C_{1m_0} \\ C_{21} & C_{22} & \dots & C_{2m_0} \\ \dots & \dots & \dots & \dots \\ C_{m_01} & \dots & \dots & C_{m_0m_0} \end{bmatrix} \quad (3.8)$$

$C$  represent the total CSM where  $m_0$  is the total amount of microphones in the array. In conventional beamforming the output spectrum is given by the equation 3.9.

$$Y(w) = \frac{w^T C w}{m_0^2} \quad (3.9)$$

Where  $w$  is the steering vector,  $T$  as superscript implies complex transpose and  $m_0$  is the total amount of microphones in the array. This expression can be extended in order to include weighting of individual microphones or diagonal removal of the CSM.

One method to suppress the effect of noise on the result is to remove the auto-spectrum diagonal of the CSM. However the matrix is not positive definite anymore as the eigenvector might be negative and the side lobes in the final source map can be of negative values, which does not make sense in the physical world. The negative side lobes can interrupt weaker sources so that they are not identified [11].

## 3.2 DAMAS

DAMAS stands for "deconvolution approach and mapping of acoustic sources" and was developed by Brooks and Humphrey at NASA Langley Research Center in 2004 [3]. Essentially DAMAS is a post processing method to further increase the accuracy of the source map generated by beamforming. A drawback of beamforming in general is the strong presence of side lobes which deconvolution algorithms such as DAMAS tries to suppress. The process begins with the computation of the conventional beamforming results for all points of a grid. DAMAS is a deconvolution approach that solves a series of linear equations in order to gain a better source map resolution [3]. In order to arrive with such a solution a problem definition is useful.

$$P_{m:n} = Q_n e_{m:j}^{-1} \quad (3.10)$$

Where  $P_{m:j}$  is the pressure transform of microphone  $m$  is related to a modeled source at position  $j$ .  $Q_j$  is the pressure transform of environmental parameters and  $e_{m:j}^{-1}$  is a model of a propagated signal to actually render the transmission of  $P_m$ . Equation 3.10 now yields a CSM that looks a little bit different.

$$G = X_j \begin{bmatrix} (e_1^{-1}) * e_1^{-1} & (e_1^{-1}) * e_2^{-1} & \dots & (e_1^{-1}) * e_{m_0}^{-1} \\ (e_2^{-1}) * e_1^{-1} & (e_2^{-1}) * e_2^{-1} & \dots & \dots \\ \dots & \dots & \dots & \dots \\ \dots & \dots & \dots & (e_{m_0}^{-1}) * e_{m_0}^{-1} \end{bmatrix} \quad (3.11)$$

Where  $X_j$  is the mean square pressure per bandwidth for each microphone  $m$  and normalize for distance. Now the total modeled cross spectral matrix can be obtained.

$$G_{mod} = \sum_j G_{j_{mod}} \quad (3.12)$$

From equation 3.9 a new expression is obtained:

$$Y_{j_{mod}}(\hat{e}) = \left[ \frac{\hat{e}^T G_{mod} \hat{e}}{m_0^2} \right]_j \quad (3.13)$$

It is now time to merge equations 3.11, 3.12 and 3.14 which yields:

$$Y_{j_{mod}}(\hat{e}) = \sum_{j'} \frac{\hat{e}_j^T [ ]_j \hat{e}_j}{m_0^2} X_{j'} \quad (3.14)$$

Where the  $[ ]_j$  denotes the modeled CSM from equation 3.11. Finally an expression which can be solved is found.

$$Y_{j_{mod}}(\hat{e}) = A X_j \quad (3.15)$$

Where matrix A consists of the following components:

$$A_{jj'} = \frac{\hat{e}_j^T [ ]_j \hat{e}_j}{m_0^2} \quad (3.16)$$

The system of linear equations can now be solved iteratively for all sources  $N$  in the source map  $X_n$  with the following expression.

$$X_j = Y_j - \left[ \sum_{j'=1}^{j-1} A_{jj'} X_{j'} + \sum_{j'=j+1}^N A_{jj'} X_{j'} \right] \quad (3.17)$$

### 3.3 CLEAN

In June, 1974, J.A. Högbom published "Aperture Synthesis With A Non-Regular Distribution Of Interferometer Baselines" [1]. At that time, situated at the observatory in Stockholm, Högbom commenced the work to tackle the issues with

astronomic images using radio interferometric telescopes. Radio interferometry was a well established procedure at this time which included theorems in the area of Fourier optics. Unfortunately there was no way to avoid the higher spatial frequencies. Essentially this meant extensive synthesis for interferometers in order to generate astronomic images. Of course astronomers wanted to go faster and to be able to measure numerous astronomic sources. Högbom gathered data from various such sources at the Green Bank Interferometer [1]. He was contemplating on how to generate an image from the collected data and tried several approaches. Ultimately this led to the development of the first iterative CLEAN approach.

The original CLEAN algorithm worked as following:

- Obtain data using radio interferometric telescopes.
- Locate the strongest source.
- Remove part of the strongest source according to the previously determined loop gain from the "dirty image" using the calculated PSF.
- Replace the "dirty image" with the one where strongest source is removed and repeat the process until the side lobes have been heavily reduced and a clean representation of the sources is acquired.

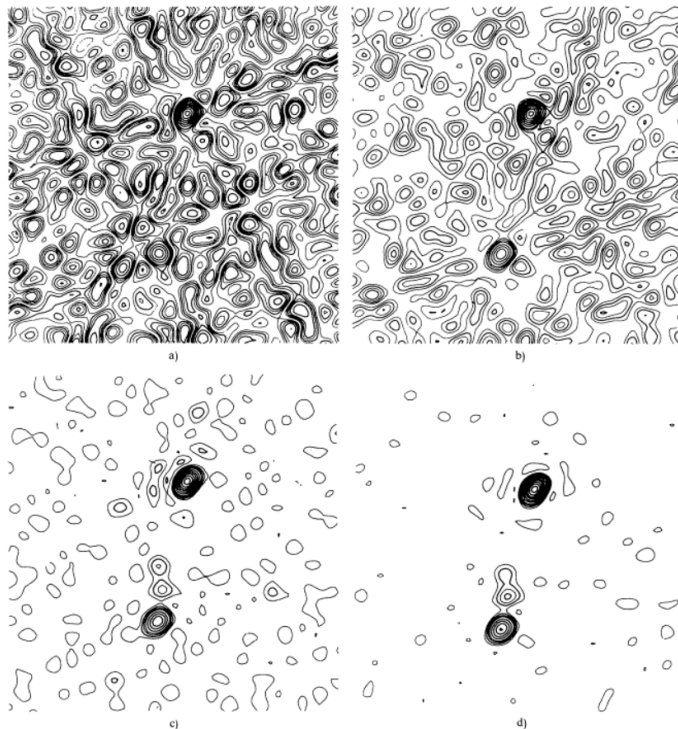


**Figure 3.2:** CLEAN algorithm applied on radio source 3C 244.1 where a) is the dirty map at first iteration and b) is the clean map at first iteration.  $\gamma = 1$  is used in this illustration. c) is the clean map at second iteration and d) is the clean map result after six iterations. Image source: [1]

As the CLEAN algorithm is reducing the the side lobes and other noise from the image, the algorithm converges to a desired result. An image of astronomic sources

is mainly empty and the algorithm only has a few source points to identify, as one could imagine. Högboms CLEAN algorithm is considered ahead of its time and has, since its discovery, been modified and optimized to be useful even outside of astronomic imaging. In figure 3.2 an example of the original CLEAN algorithm can be seen.

### 3.4 CLEAN-SC

A more recent version of the traditional CLEAN is the so called CLEAN-SC, SC stand for source coherence. This is a frequency domain deconvolution approach developed by Sijtsma and is mainly developed for acoustic imaging. CLEAN-SC manages to suppress the impact of the PSF by using spatial coherence between the actual sources and side lobes [5]. Much like the traditional CLEAN algorithm the CLEAN-SC follows a similar procedure.

- Obtain a Cross Spectral Matrix (CSM).
- Calculate coherence parts for a each grid point of the CSM.
- A copy of the CSM used for iterative calculations is assigned to a so called dirty map
- Locate the strongest source and delete the coherent parts from the dirty map.
- Add the strongest source to an empty copy of the dirty map, commonly referred to as clean map.
- Repeat until convergence is reached or another stop criteria, like a set amount of iterations.

Once CLEAN-SC is finished a clean map is obtained with clearly suppressed side lobes leaving the strongest source to be observed in higher detail. It works because we can assume that the CSM can be defined as a sum of supplements from  $K$  amount of incoherent sources [11].

$$C = \sum_{k=1}^K \langle p_k p_k^* \rangle \quad (3.18)$$

Where  $p_k$  is a acoustic source vector of arbitrary length which represent the Fourier transformed signal. In order for equation 3.18 to valid it must abide by following conditions:

- All sound sources must be incoherent
- No appended incoherent noise
- The signal from the same source must not be a subject to decorrelation between microphones. Environmental conditions can cause such issues.
- Diagonal deletion of the CSM can be implemented and neglect auto spectrum.

Just as in traditional CLEAN algorithm, CLEAN-SC primarily locates the strongest source by making use of steering vectors in the mesh grid where  $\xi_j$  is the current grid point. In order to find the strongest source in the beamforming, following expression is obtained.

$$\max(A) = A(\xi_j) = w_j^* C w_j \quad (3.19)$$

$A(\xi_j)$  is the estimated source power and  $w_j$  is the weight vector which is calculated by the steering vector  $g_k$ . The steering vector itself is obtained by equation 3.20.

$$g_n = \frac{-\exp(-2\pi i f \|\vec{x}_n - \vec{\xi}\|/c)}{4\pi \|\vec{x}_n - \vec{\xi}\|} \quad (3.20)$$

Where  $f$  is the frequency,  $c$  the speed of sound,  $x_n^{\rightarrow}$  the position of the microphone and  $\xi^{\rightarrow}$  the source location. The reciprocal source component  $h_j$  can be explained by:

$$h_j = \frac{C w_j}{A(\xi_j)} \quad (3.21)$$

By inserting equation 3.18, the following expression is obtained:

$$h_j = \frac{\sum_{k=1}^K (\frac{1}{2} p_k^* w_j) p_k}{A(\xi_j)} \quad (3.22)$$

Given that there is enough distance between the sources, the term inside the parenthesis in equation 3.22 will be large and a good estimate of the peak source while small for other sources. This means that the source component is a fair appraisal of the loudest source vector, leading to the final expression:

$$h_j = \frac{(A(\xi_j))^2 h_j h_j^*}{|p_k^* w_j|^2} \approx A(\xi_j) h_j h_j^* \quad (3.23)$$

Which is the component that should be subtracted from the dirty map in each iteration until a set of iterations are done or other stop criteria is met. The whole process can be summarized to the following expression:

$$C = \sum_{i=1}^I A_{\max}^{(i-1)} h^{(i)} h^{*(i)} + D^{(i)} \quad (3.24)$$

Where  $C$  is the original CSM,  $\sum_{i=1}^I$  determines the sum over number of iterations,  $A_{\max}^{(i-1)} h^{(i)} h^{*(i)}$  is the clean map and  $D^{(i)}$  is the dirty map.

Some benefits of the CLEAN-SC is that it does not depend on any PSF, it counteracts negative side lobes, relatively fast and can remove sources from outside the grid. On the other hand it performs rather poorly when decorrelation occurs, for instance outdoors measurements where there is a great distance between source and microphone array [5].

### 3.5 CLEAN-T

CLEANT is the most recent modification that came from the original CLEAN algorithm. The algorithm was developed by Cousson et al. [8] and is a time domain deconvolution approach. This approach has previously been tested on high speed train and rotating sound sources by Kujawski [10], Sarradj and Cousson et al. Previously

mentioned researchers have made extensive studies to demonstrate that CLEAN provides more accurate results for localization and quantification of moving sources than previously incorporated methods. Like many other algorithms, CLEAN is a deconvolution approach with the goal to remove the influence of the PSF and obtain the original condition of the source map. CLEAN is using the resulting source map from time domain beamforming to initiate the dirty map, therefore this approach requires time domain beamforming to be performed before commencing the deconvolution algorithm. The results from beamforming in time domain can be obtained with Eq. 3.2. CLEAN will locate the strongest source in the dirty map for every iteration and subtract the effect of this source from the microphone signals until a stop criteria is met. Following process is the initial condition of the CLEAN approach:

- $\Phi^{(0)}(t, x_j) = b(t, x_j, \{p_m\})$ . This is simply the dirty map being initiated with the beamforming result.
- $\Gamma^{(0)}(t, x_j) = 0$ . The clean map is initiated with zeros in the same size and shape as the dirty map.
- $p_m^{res(0)}(t) = p_m(t)$ . The parameter representing the residual microphones is initiated with the original microphone signals.

The next step is to locate the strongest source within the dirty map. This is done for every iteration as well and can be obtained by integrating over a time frame  $T$  for focus point  $\hat{x}_j$ . A mathematical equation for this process is presented as

$$\hat{x}_j = \arg \max_{\hat{x}_j} \int_T |\Phi^{(i-1)}(t, x_j)|^2 dt \quad (3.25)$$

The strongest source is then also added to the clean map.

$$\Gamma^{(i)}(t, \hat{x}_j) = \Gamma^{(i-1)}(t, \hat{x}_j) + \gamma \Phi^{(i-1)}(t, \hat{x}_j) \quad (3.26)$$

$\gamma$  represents the loop gain and is commonly set to a value between  $[0, 1]$ . By using  $\gamma$  the amount of added signal can be scaled. At this stage of the algorithm a modeled microphone signal from the strongest source  $\hat{x}_g$  is created.

$$p_m^{res(i)}\left(t + \frac{r_{x_j m}}{c}\right) = p_m^{res(i-1)}\left(t + \frac{r_{x_j m}}{c}\right) - \gamma \frac{\Phi^{(i-1)}(t, \hat{x}_j)}{r_{\hat{x}_j m}(t)(1 - M \cos \theta_{\hat{x}_j m}(t))^2} \quad (3.27)$$

After this step the new microphone signal,  $p_m^{res(i)}\left(t + \frac{r_{x_j m}}{c}\right)$ , is used to perform beamforming again and the whole process is repeated for a set amount of iterations. Another stop criteria that can save computation cost is when there is an increase of energy in the beamforming results from the residual microphone signal. The outcome of CLEAN is a clean map representing the identified sources. The sum of all identified sources can be expressed by equation 3.28

$$\Gamma(t, x_j) = \gamma \sum_{k=1}^K \Phi^{(k)}(t, x_j) = \gamma \sum_{k=1}^K b(t, x_j, \{p_m^{res(k)}\}) \quad (3.28)$$

Where  $K$  is the total amount of iterations of the CLEAN algorithm.

## 3.6 Implementation

The whole implementation builds on the code base that DLR had previously developed. It contains delay-and-sum beamforming as well as the DAMAS deconvolution algorithm among other necessary processing tools like resampling. CLEAN-T builds on time domain beamforming which is already performed by the software of DLR. Apart from beamforming code, DLR provided measured data, recorded trajectory of the aircraft and code for constructing the grid. All other functions were developed in this thesis. Several processing steps that previously existed require some modification to suit the CLEAN-T approach. The entire implementation was done in Python with the use of external libraries. Below pseudo-code is used to describe the implementation of the CLEAN-T algorithm.

1. Specify interval of observation (angle in degrees from the array reference point), aircraft trajectory and size of mesh grid that follows the aircraft trajectory.
2. Load recorded data or simulated data as microphone signal which will be used by the algorithm.
3. Set a number of maximum iterations and loop gain.
4. Create a butterworth bandpass filter of order six with cutoff frequencies at 100 Hz and 10000 Hz. This can be useful due to beamforming limitations in frequency resolution and focuses in on the most common frequencies emitted by aircraft.
5. Filter the microphone array signal.
6. Commence the algorithm loop for a set amount of iterations. The other stop criteria is when the energy within the dirty map at a certain iteration increases. Meaning that the strongest sources have been treated and noise is mainly the remnants.
7. Perform beamforming in time domain and collect the emission times for the sound sources. This is done by removing geometric attenuation and then delay and sum beamforming. The signal is downsampled before performing beamforming to save computation costs.
8. Assign the result from beamforming to dirty map.
9. Initiate a clean map in the same size and shape as the dirty map.
10. Obtain all potential sources by creating an array with all points from the mesh grid that follows the aircraft trajectory.
11. Call sourcemap object for future design of the actual acoustic image from the clean map.
12. Find max index in dirty map. The index points the location within the dirty map where the strongest source is located.
13. Add the strongest located source signal from the dirty map into the clean map using the loop gain to scale the amount added.
14. Create a trajectory for only the strongest source located in the dirty map. This saves computation cost by only taking one certain point into account instead of all possible sources at every grid point.
15. Calculate the propagation time from the strongest source to each microphone.

16. By combining the emission times with the propagation times, the receiving times can be calculated.
17. Now that the receiving times are known for the microphone array, the interval of recording times can be found with the same high sampling frequency as the recorded signals. This time array is saved for the modeled microphone signal. The time array matches the angle interval of interest in which recording is performed.
18. Calculate the doppler attenuation as well as the distance attenuation from the strongest source to each microphone.
19. Use the attenuation coefficient to calculate the sound pressure of the strongest source at receiving position of each microphone. This is done for the entire duration of the recording. Notice that this signal is still down-sampled as a consequence of beamforming.
20. Interpolate the modeled microphone signal by using the resampled time interval to get a modeled microphone signal that matches the sampling frequency of the recorded signals.
21. Remove the modeled microphone signal from the recorded microphone signals.
22. Pass the microphone signals with the strongest source removed as the original microphone signal for the next iteration.
23. Go to step 7 to perform beamforming with the new microphone signal and repeat the process until stop criteria is met.
24. Plot clean map

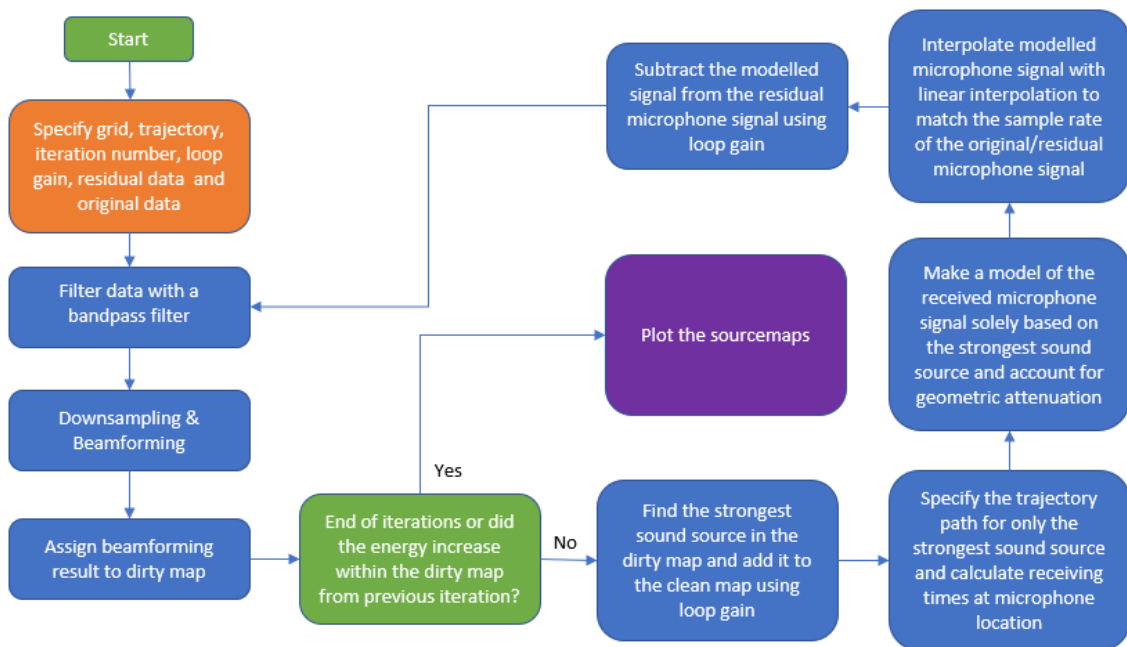


**Figure 3.3:** A flow chart representing the code structure of the CLEAN implementation.

# 4

## Results

In this chapter the final sourcemaps generated by the CLEAN algorithm will be presented. The two sourcemaps which will be presented is the Clean Map, generated by CLEAN and the Dirty Map, generated by beamforming. Several datasets have been used, two simulated overflying measurements, received by Swiss EMPA, which can be seen in figure 4.1. The real measurements are from 2016 and 2019 and were performed at the private airport of DLR with their microphone array, seen in figure 4.2. Several settings have been tested, such as, different values for the loop gain ( $\gamma$ ), diagonal removal activated/deactivated and single third octave band implementation of source localization. At last a comparison between CLEAN and DAMAS will be presented by the results of the real overflying measurements in order to determine the pros and cons of the two approaches. All color bars represents the sound source levels in dB SPL.

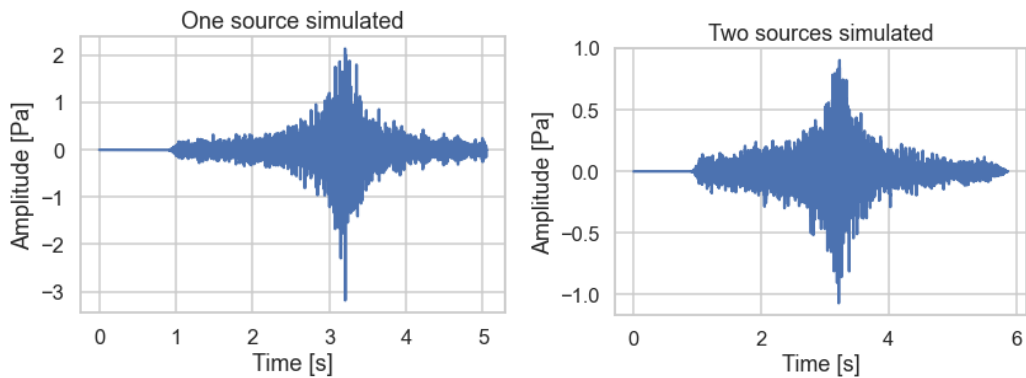


**Figure 4.1:** (Left): Simulated flyover measurements of a single monopole source (Right): Simulated flyover measurements of two monopole sources. Both figures show mean value of all microphones.

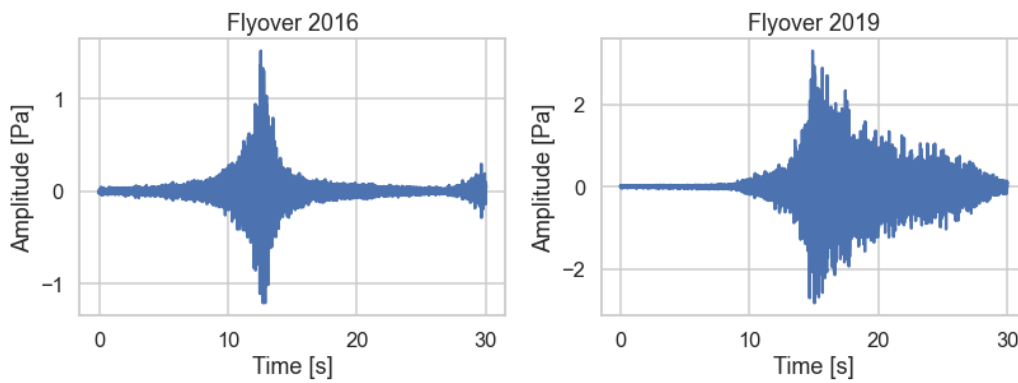


**Figure 4.2:** (Left): Real flyover measurements performed in 2016 (Right): Real flyover measurements performed in 2019. Both figures show mean value of all microphones.

In the beginning of every data analysis and for every iteration of CLEANT a band-pass filter is applied to narrow down the frequency range of interest and due to limitations of beamforming.

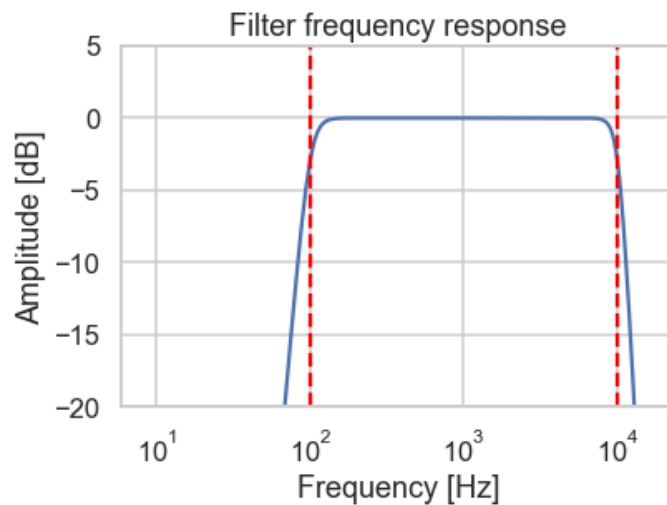


**Figure 4.3:** Butterworth bandpass filter of order 6 with cutoff frequencies at 100 Hz and 10 kHz.

## 4.1 Simulated overflying measurements of a single sound source

The first data set consist of a simulated overflying monopole source containing information in a broad frequency range. It was useful for verification process since it is a single source located in the middle of the detection area. This way it was easy to determine if the desired result was achieved.

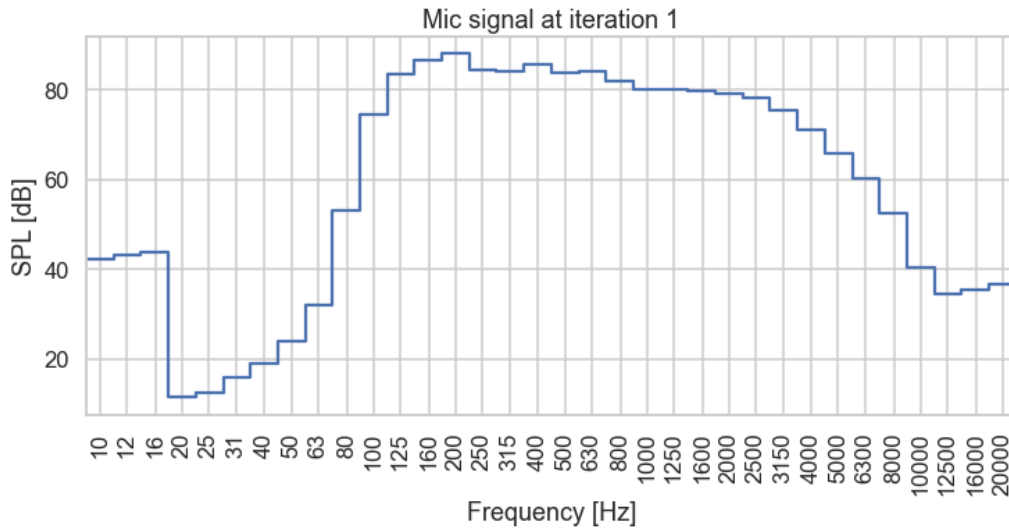


**Figure 4.4:** Simulated overflying measurement with one monopole source in TOB, only processed with the bandpass filter seen in figure 4.3.

### 4.1.1 Diagonal removal deactivated

In this section the diagonal removal of the CSM has not been activated and a  $\gamma$  value of 1 is set.

In figure 4.5 and 4.8 another source appears to the left of the real source in the middle position. This is caused by the shortcoming of beamforming and spatial undersampling. The strong sidelobes in the PSF can sometimes be identified as an additional sources.

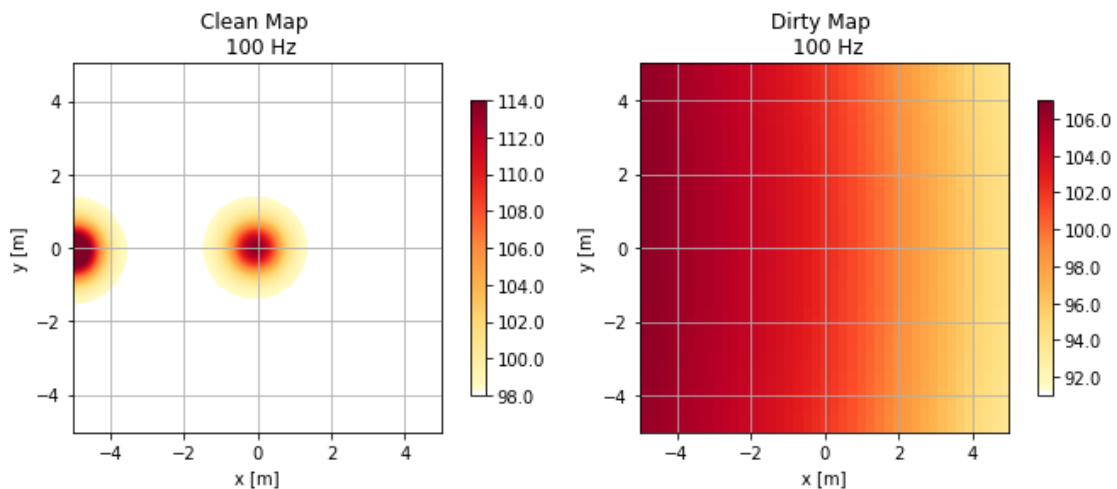


**Figure 4.5:** CLEAN results of a single monopole source at 100 Hz.

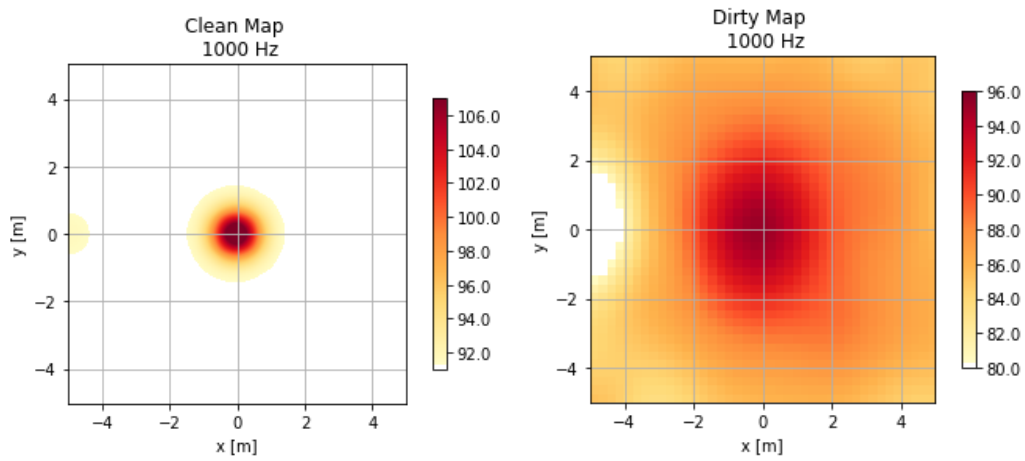


Figure 4.6: CLEAN results of a single monopole source at 1000 Hz.

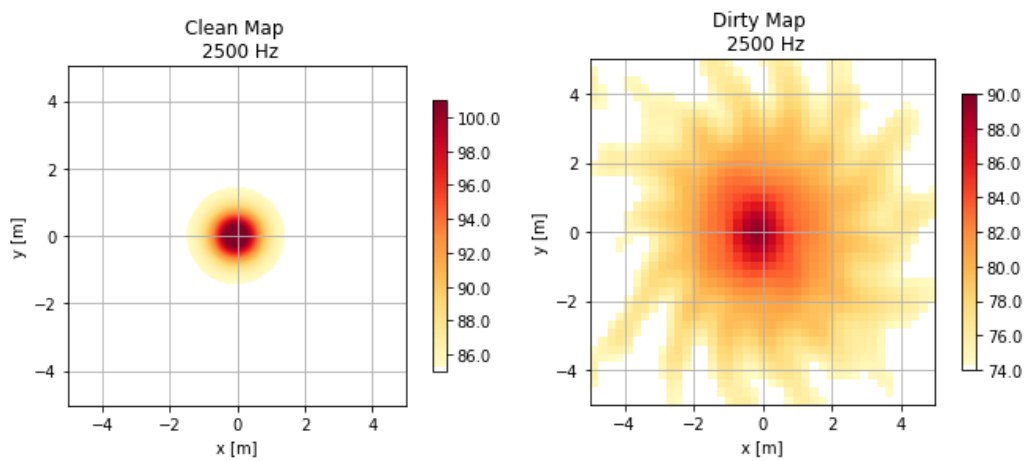


Figure 4.7: CLEAN results of a single monopole source at 2500 Hz.

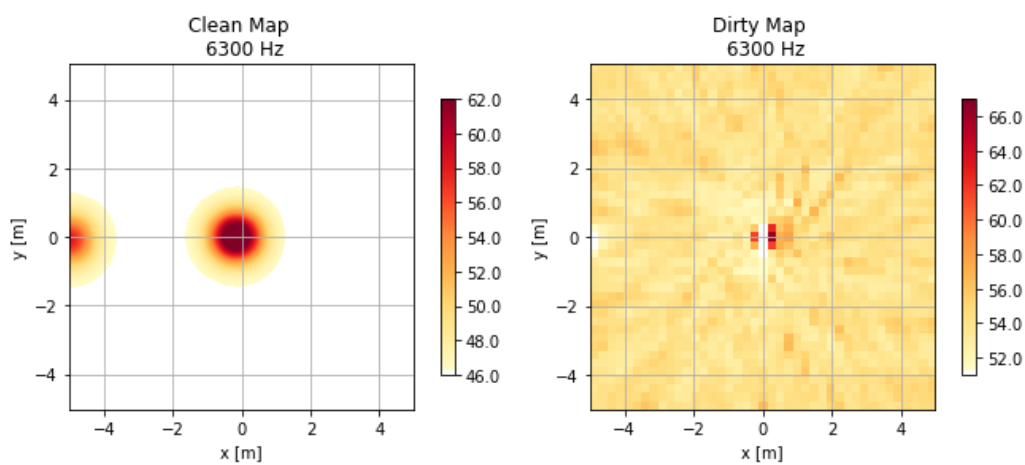
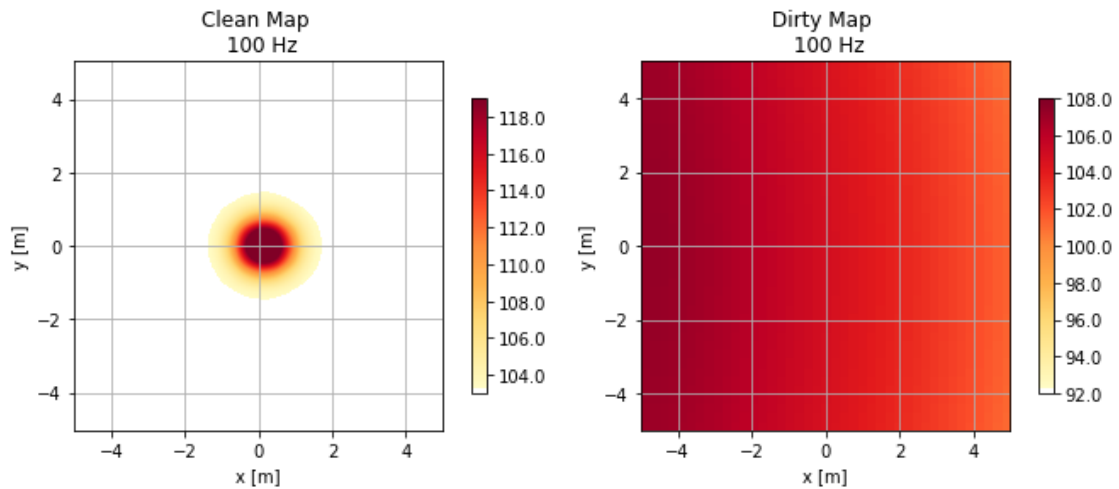


Figure 4.8: CLEAN results of a single monopole source at 6300 Hz.

### 4.1.2 Diagonal removal activated

In this section the diagonal removal of the CSM is active and a  $\gamma$  value of 1 is set.

When diagonal removal is activated the spatial accuracy is increased at the compromise of level accuracy. Comparing with previous section 4.1.1, the influence of spatial undersampling has been lowered for all frequencies. The results are significantly improved with diagonal removal.



**Figure 4.9:** CLEAN results of a single monopole source at 100 Hz with diagonal removal activated.

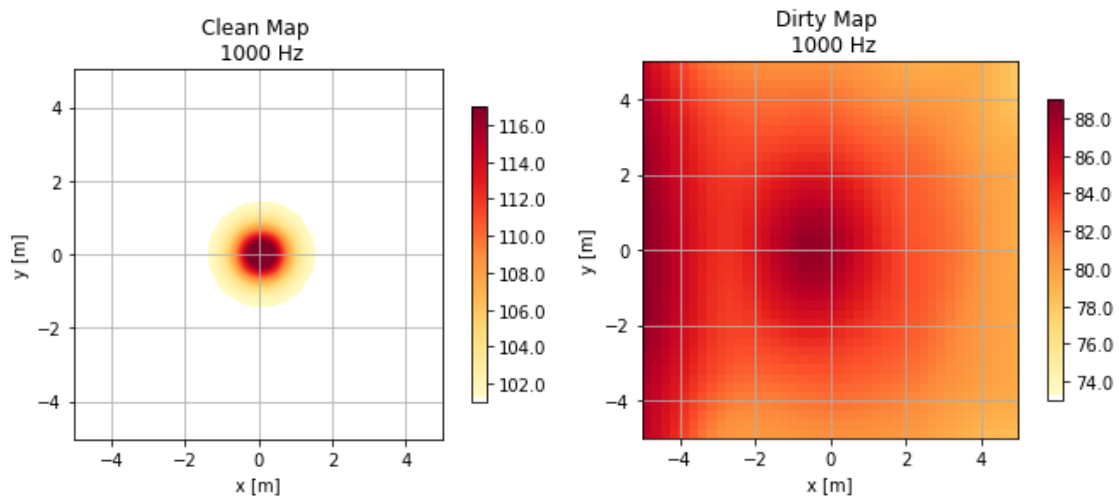


**Figure 4.10:** CLEAN results of a single monopole source at 1000 Hz with diagonal removal activated.

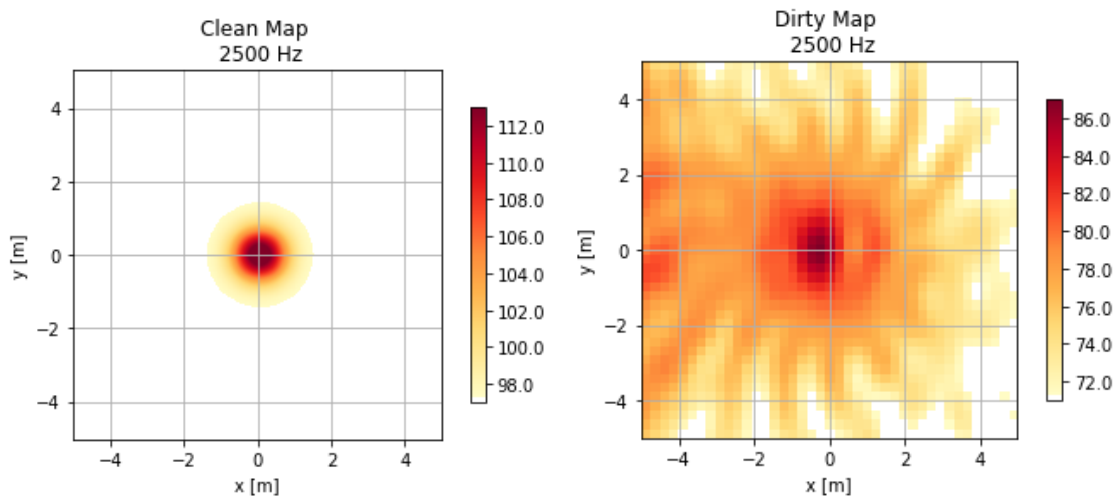


**Figure 4.11:** CLEANT results of a single monopole source at 100 Hz with diagonal removal activated.

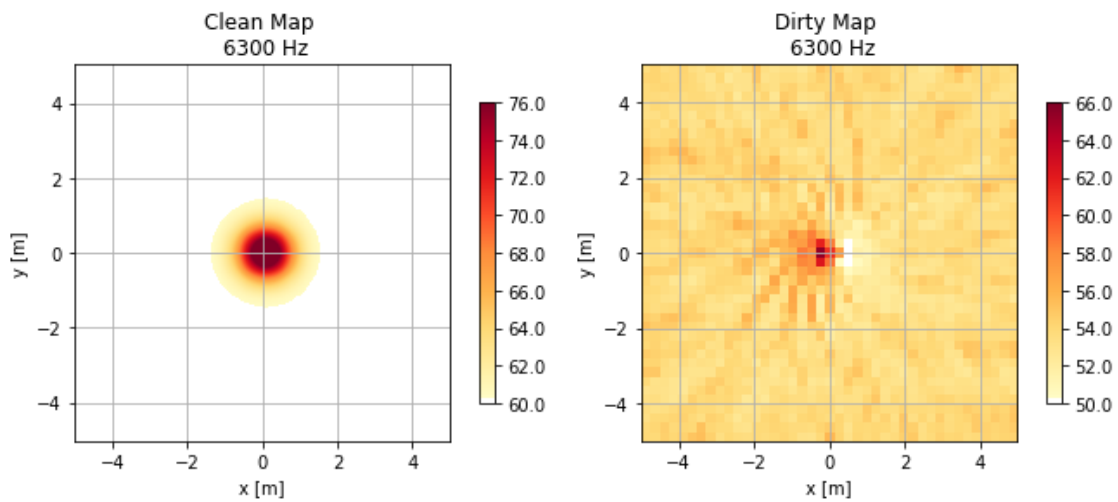


**Figure 4.12:** CLEANT results of a single monopole source at 100 Hz with diagonal removal activated.

## 4.2 Simulated overflying measurements of two sound source

A dataset simulating overflying measurements using only two monopole sources containing information in a broad frequency range. This data was also used for verification purposes in order to investigate if the CLEANT algorithm can handle several sources and what settings are optimal.

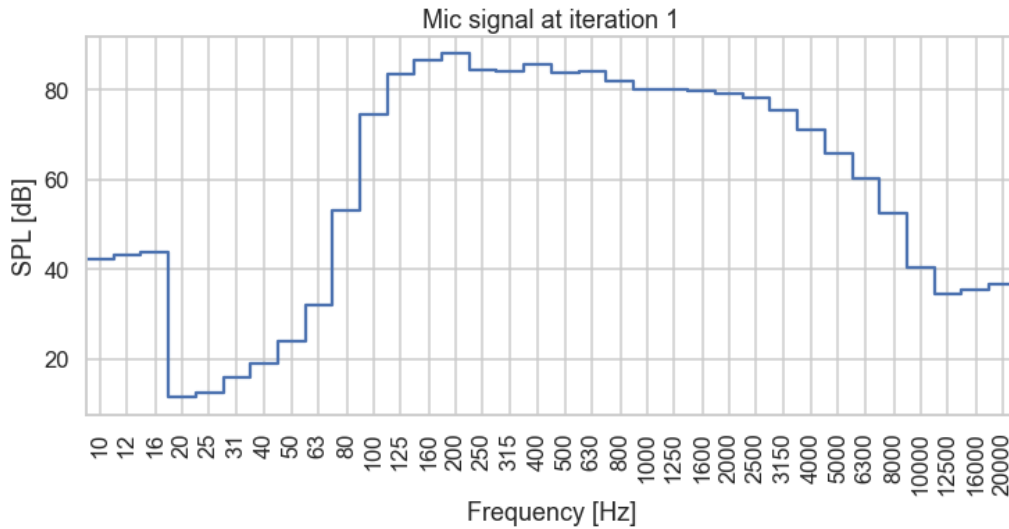


**Figure 4.13:** Simulated overflying measurement with two monopole sources in TOB, only processed with the bandpass filter seen in figure 4.3.

#### 4.2.1 Diagonal removal deactivated

In this section the diagonal removal of the CSM has not been activated and a  $\gamma$  value of 0.6 is set.

In this dataset there are two sources, one located in the middle and the other one to the right of the center positioned one. With basic parameter settings the algorithm has a hard time to identify both sources as can be seen in figures 4.14, 4.15, 4.16 and 4.17. The reason for this might be that the two sources are identical and overlap when detecting the strongest source in the dirty map.

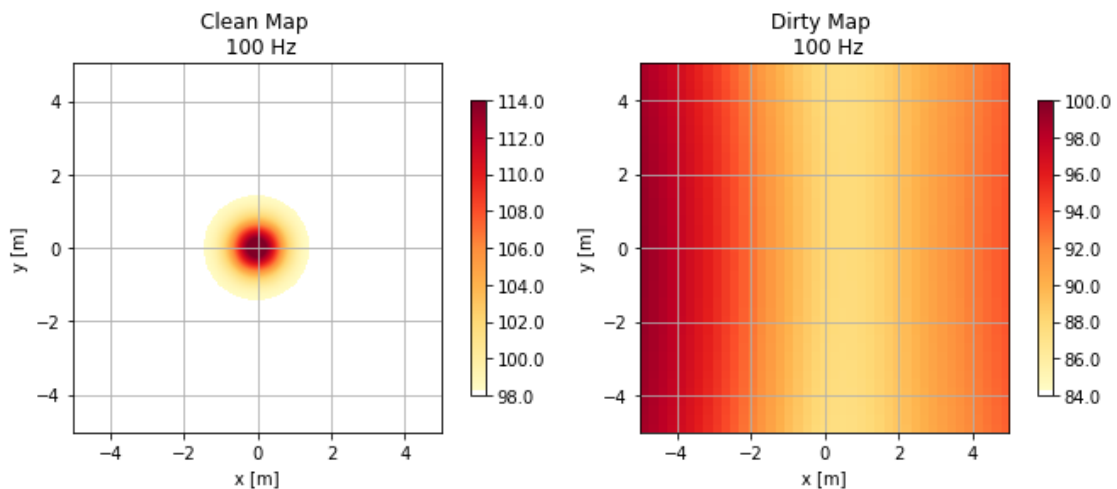


**Figure 4.14:** CLEAN results of two monopole sources at 100 Hz

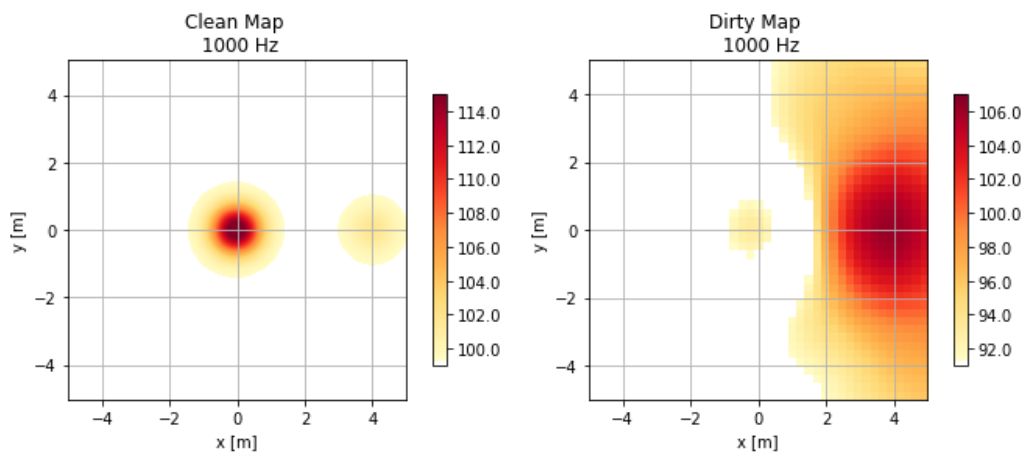


Figure 4.15: CLEANT results of two monopole sources at 1000 Hz

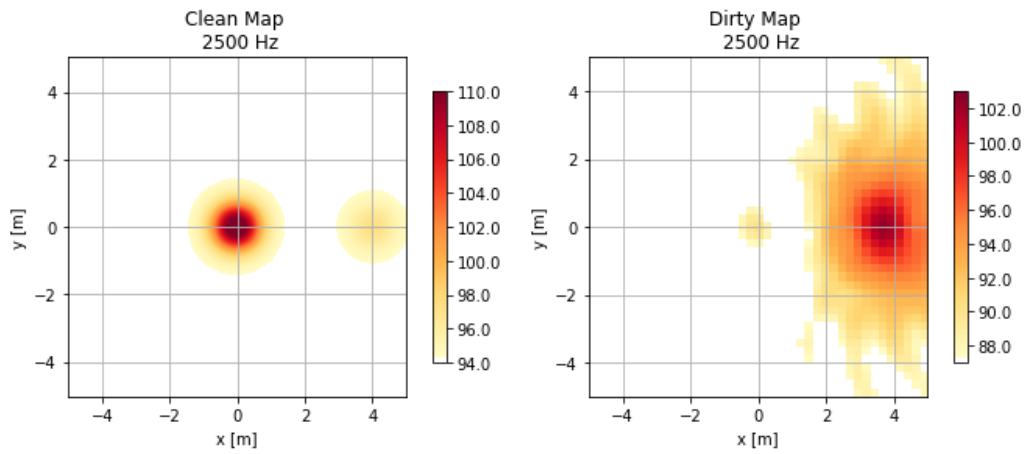


Figure 4.16: CLEANT results of two monopole sources at 2500 Hz

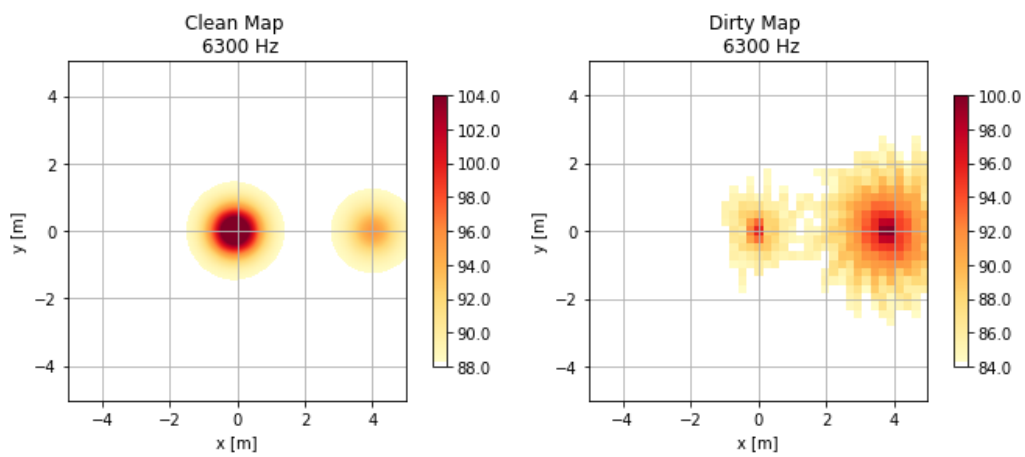
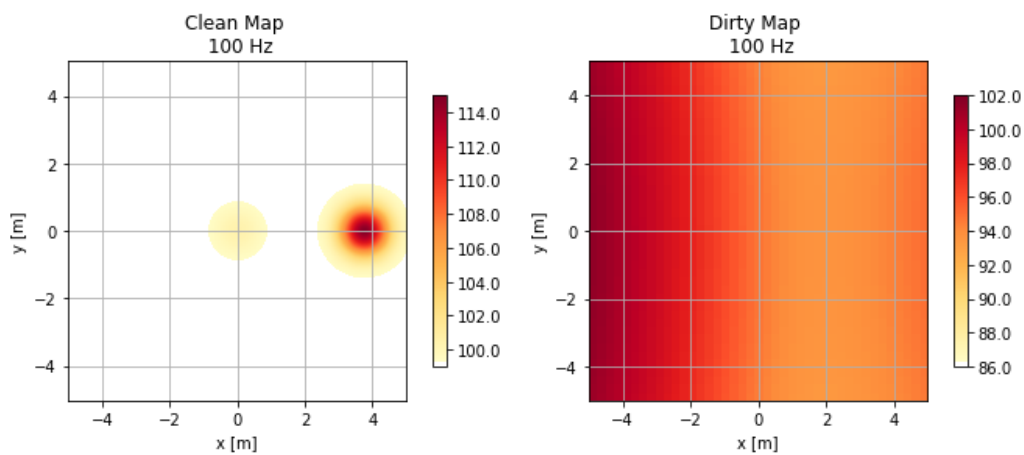


Figure 4.17: CLEANT results of two monopole sources at 6300 Hz

### 4.2.2 Diagonal removal activated

In this result section the diagonal removal of the CSM is activated and a  $\gamma$  value of 0.6 is set.

When diagonal removal is enabled the results look much better across the frequency range as both sound sources can be detected properly. In figure 4.18 there are still complications fully detecting both sources. Low frequencies are more often more affected to spatial undersampling due to the long wavelengths and therefore not accurately located.



**Figure 4.18:** CLEAN results of two monopole sources at 100 Hz with diagonal removal activated.

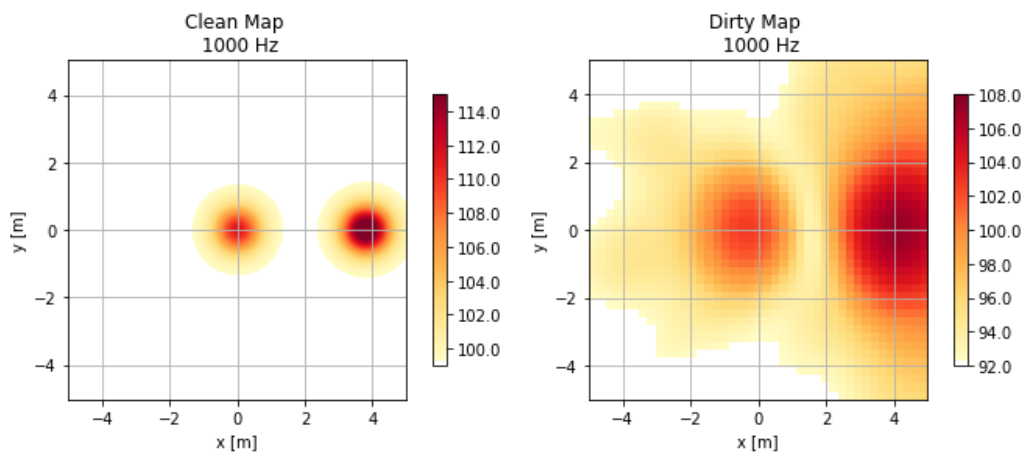


**Figure 4.19:** CLEAN results of two monopole sources at 1000 Hz with diagonal removal activated.

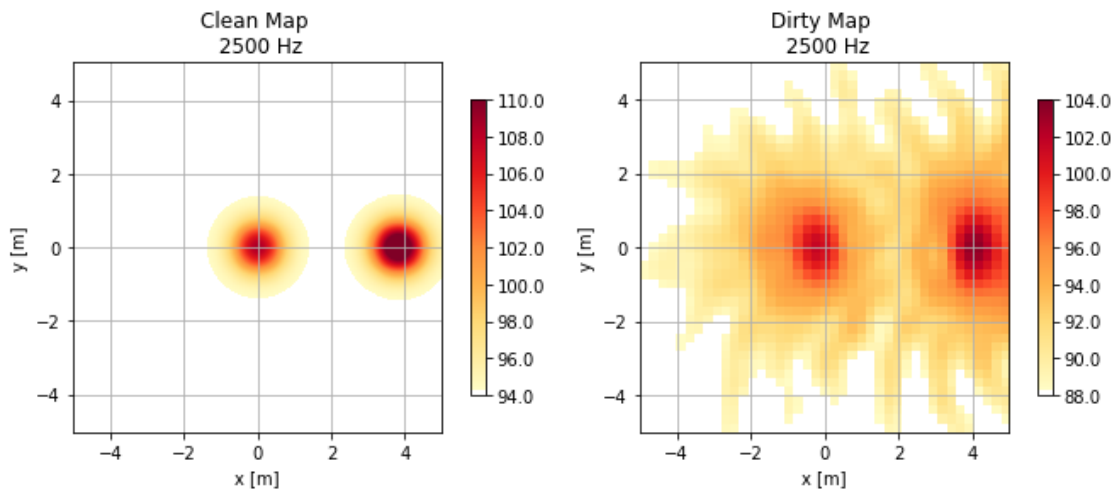


**Figure 4.20:** CLEAN results of two monopole sources at 2500 Hz with diagonal removal activated.

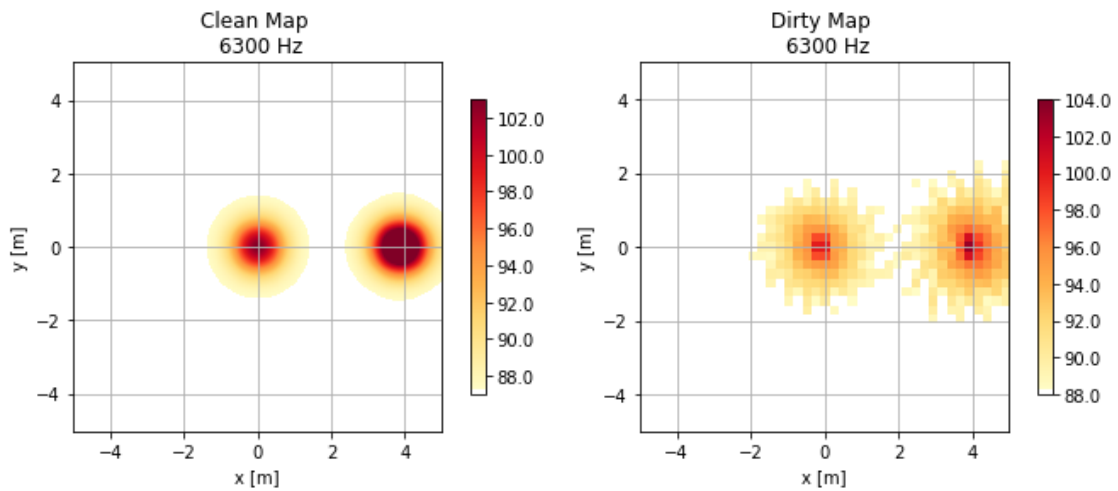


**Figure 4.21:** CLEAN results of two monopole sources at 6300 Hz with diagonal removal activated.

### 4.2.3 Diagonal removal activated and low loop gain

In this section the diagonal removal of the CSM is activated and a  $\gamma$  value of 0.1 is set.

In this setup a lower gamma value was chosen which presents less accurate results than with only diagonal removal activated. Both sources are detected, except for at 100 Hz in figure 4.22 but at a significantly lower level.

## 4. Results

---

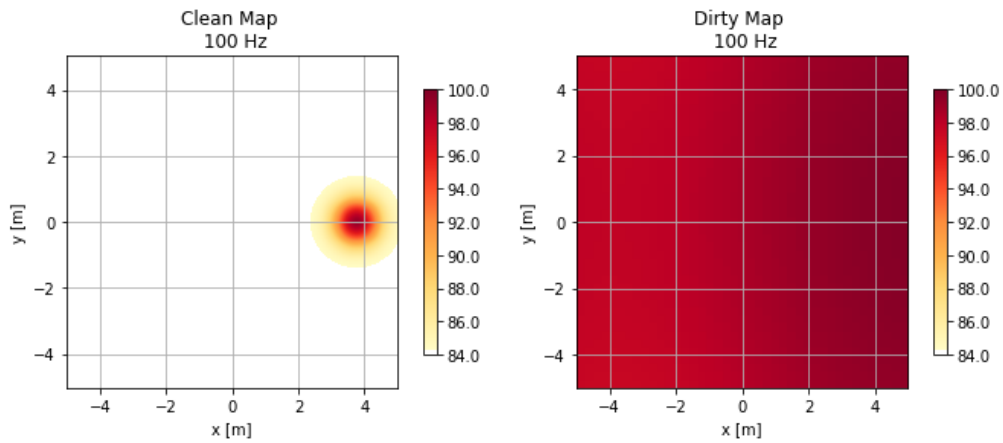


**Figure 4.22:** CLEANT results of two monopole sources at 100 Hz with diagonal removal activated and low gamma value.

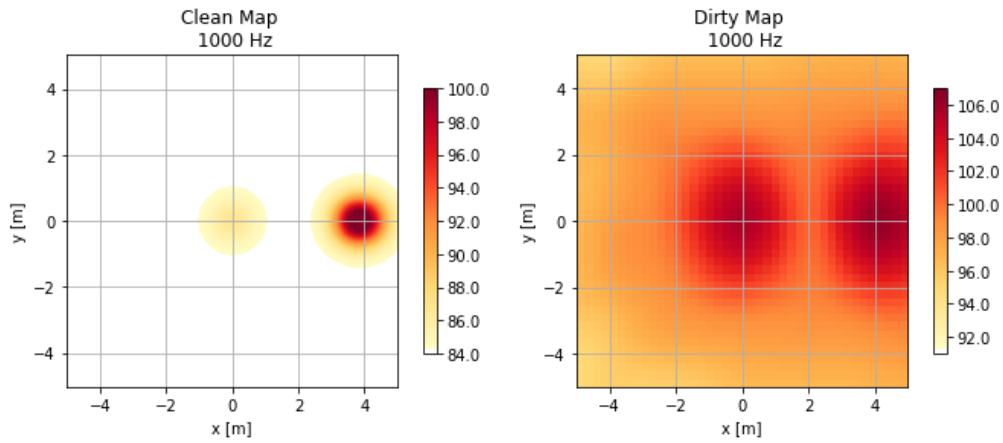


**Figure 4.23:** CLEANT results of two monopole sources at 1000 Hz with diagonal removal activated and low gamma value.

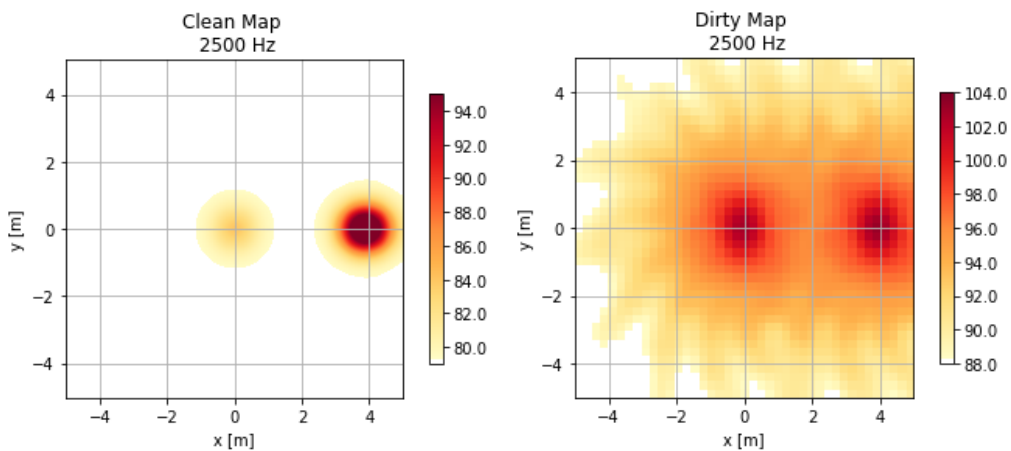


**Figure 4.24:** CLEANT results of two monopole sources at 2500 Hz with diagonal removal activated and low gamma value.

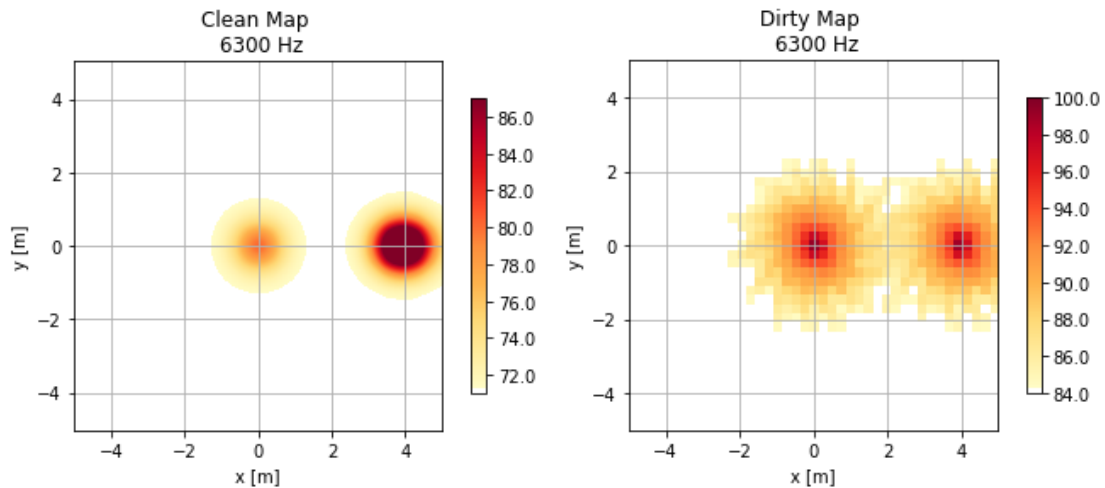


**Figure 4.25:** CLEAN results of two monopole sources at 6300 Hz with diagonal removal activated and low gamma value.

#### 4.2.4 Diagonal removal activated and single 1000 Hz TOB detection

In this section the diagonal removal of the CSM is activated and a  $\gamma$  value of 0.6 is set. The detection of the strongest source performed by the CLEAN algorithm is restricted to a single TOB of 1000 Hz.

These result show that a single TOB of 1000 Hz was not very suitable for two simulated sound sources as they are less accurate than only diagonal removal. The lack of tonal components, which single TOB detection was designed for, might be the cause.

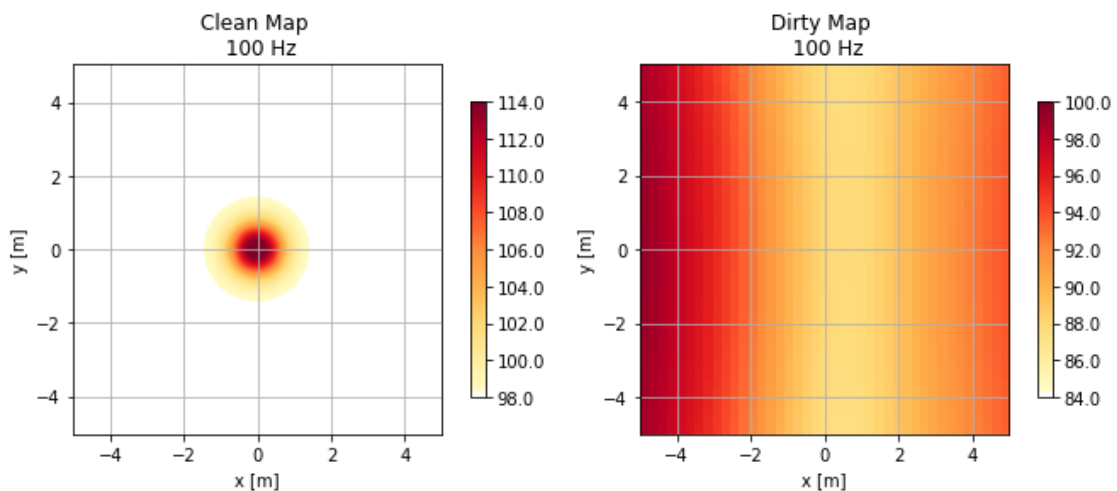


**Figure 4.26:** CLEAN results of two monopole sources at 100 Hz with diagonal removal activated and single TOB detection.

## 4. Results

---

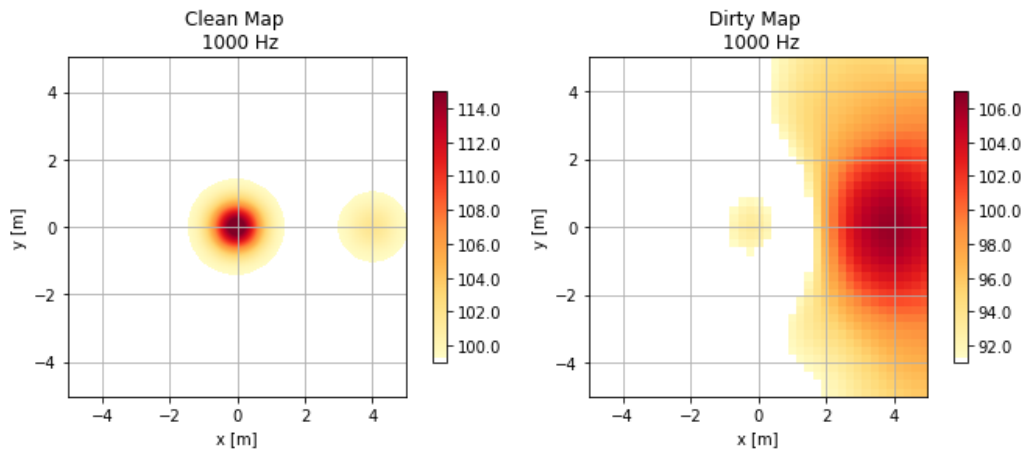


**Figure 4.27:** CLEANT results of two monopole sources at 1000 Hz with diagonal removal activated and single TOB detection.

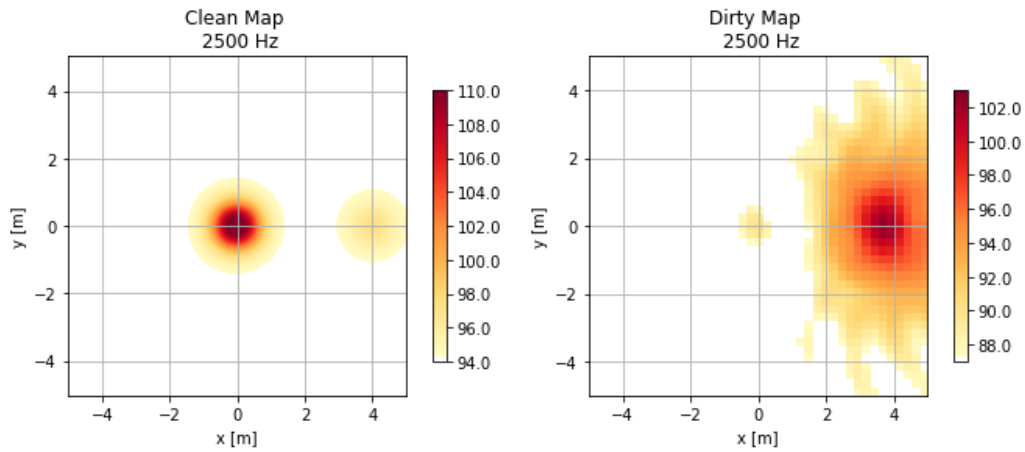


**Figure 4.28:** CLEANT results of two monopole sources at 2500 Hz with diagonal removal activated and single TOB detection.

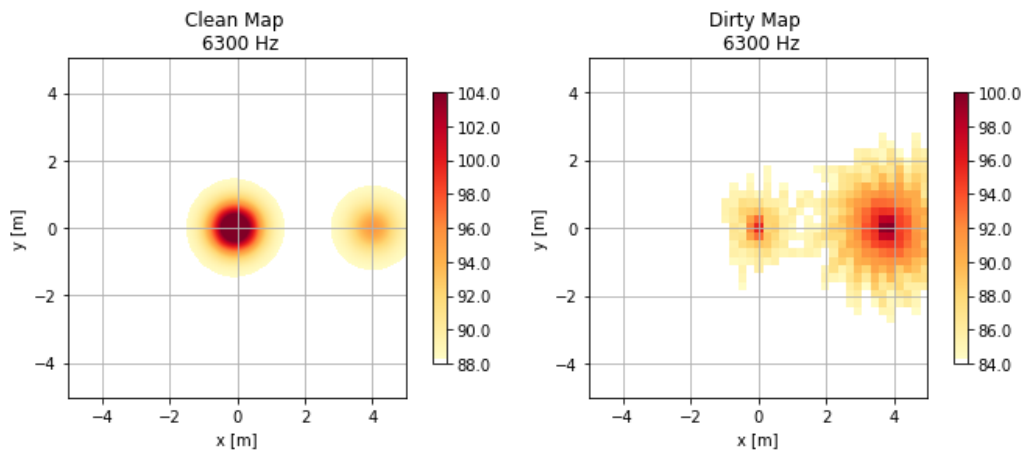


**Figure 4.29:** CLEANT results of two monopole sources at 6300 Hz with diagonal removal activated and single TOB detection.

### 4.3 Recorded overflying measurements from 2016

A more broadband noise is present in this dataset which can be observed in figure 4.30. This is due to the fact that the aircraft is approaching landing and the power of the jet engines is significantly lowered.

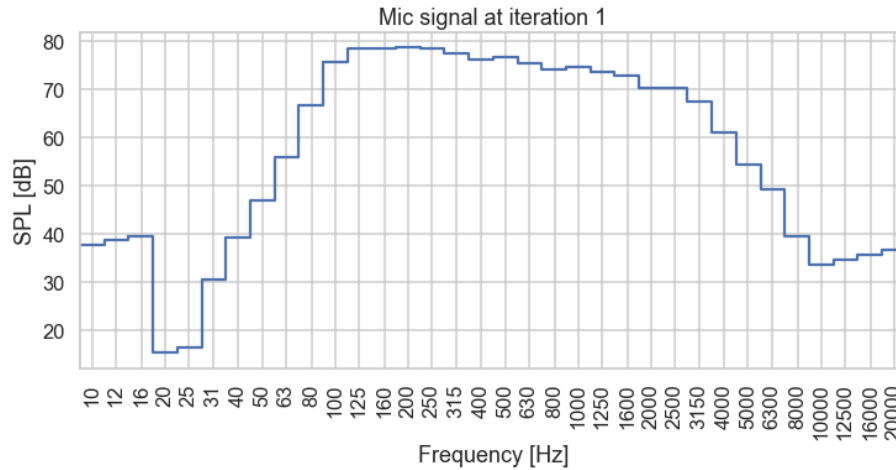


**Figure 4.30:** Recorded microphone signals in TOB only processed with the band-pass filter seen in figure 4.3.

#### 4.3.1 Diagonal removal deactivated

In this section the diagonal removal of the CSM is has been deactivated and a  $\gamma$  value of 0.6 is set.

The results reveals a lot of identified sound sources in figure 4.32, 4.33 and 4.34. These are mainly aerodynamic noises as the aircraft is approaching landing. Most of the identified sources are vortexes or turbulence caused by various sensors or parts poking out from the aircraft. At 100 Hz in figure 4.31 there are only two main sources identified behind the wings which could also be vortexes.

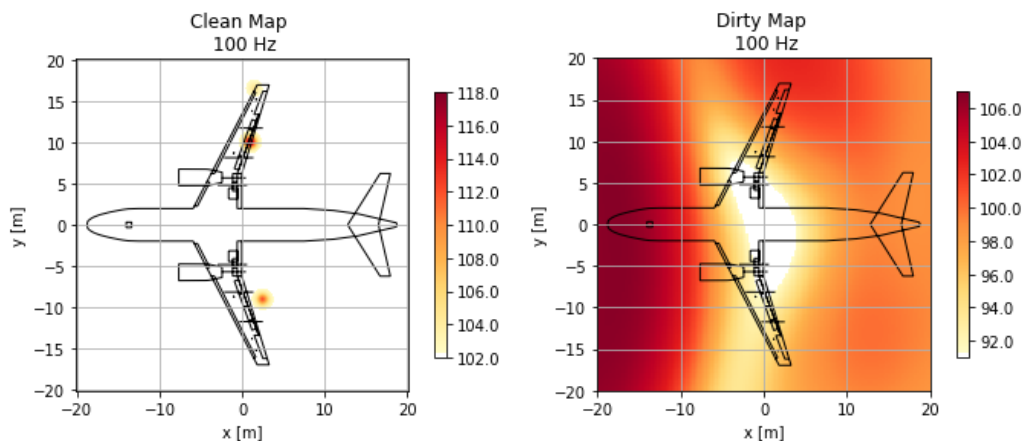


**Figure 4.31:** CLEAN results of an overflying measurement in 2016 at 100 Hz.

#### 4. Results

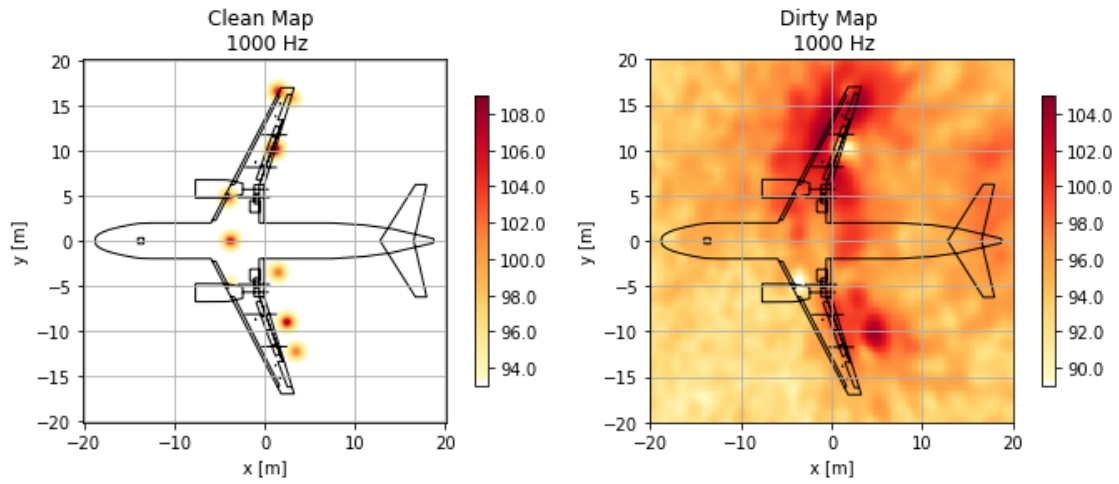


Figure 4.32: CLEANT results of an overflying measurement in 2016 at 1000 Hz.

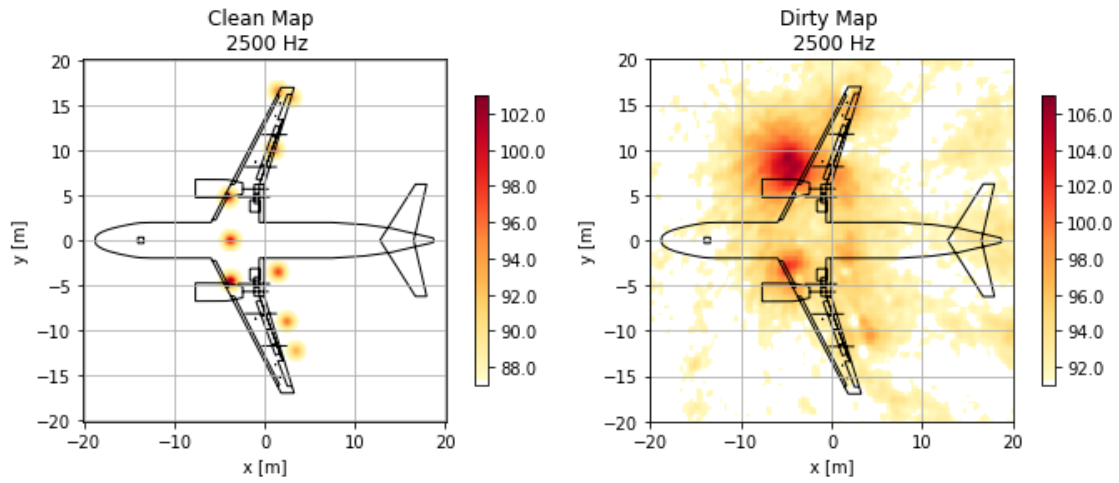


Figure 4.33: CLEANT results of an overflying measurement in 2016 at 2500 Hz.

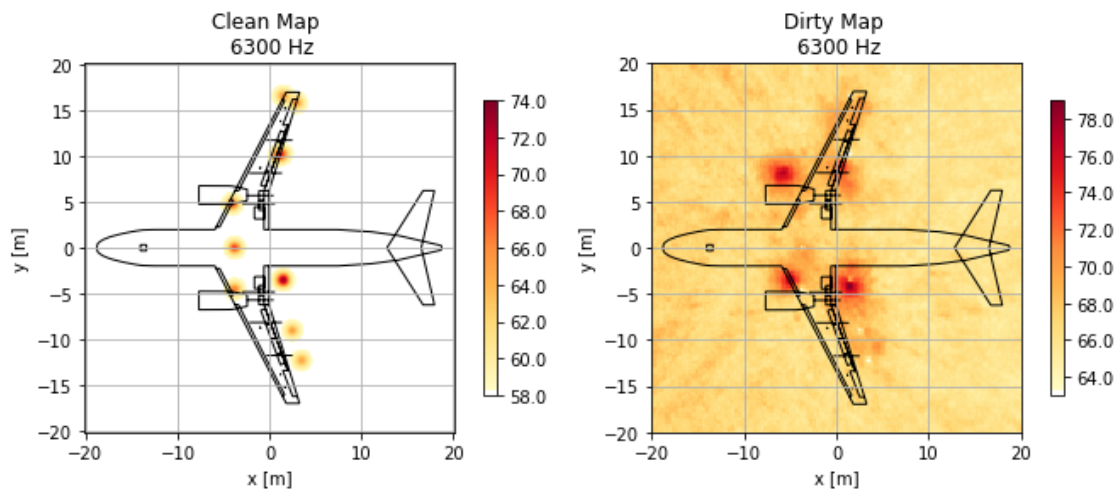
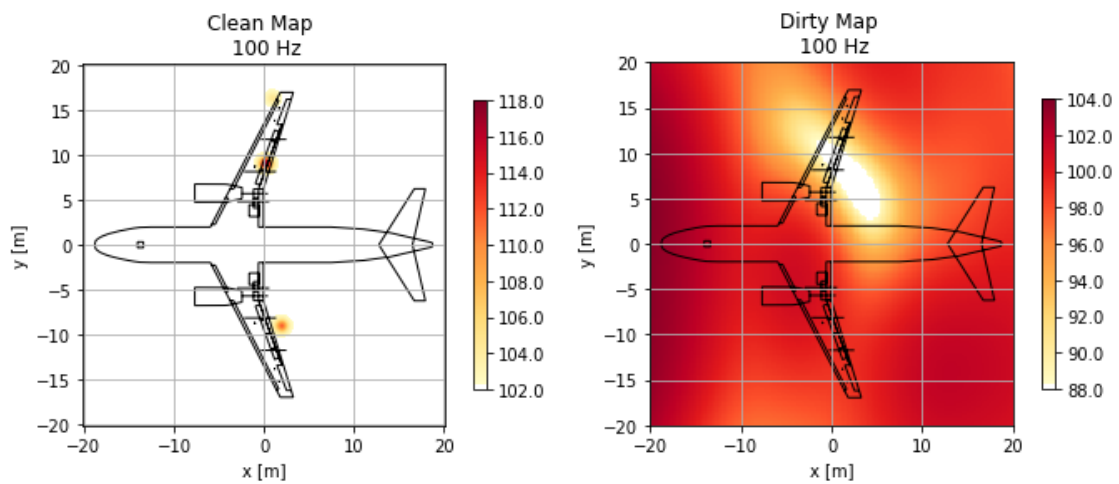


Figure 4.34: CLEANT results of an overflying measurement in 2016 at 6300 Hz.

### 4.3.2 Diagonal removal activated

In this section the diagonal removal of the CSM is active and a  $\gamma$  value of 0.6 is set.

The results with diagonal removal enabled reveals slightly better detection of sound sources around the wings. But now one of the jet engines is not fully detected. This could again be the consequence of the so called masking effect.



**Figure 4.35:** CLEAN results of an overflying measurement in 2016 at 100 Hz with diagonal removal activated.

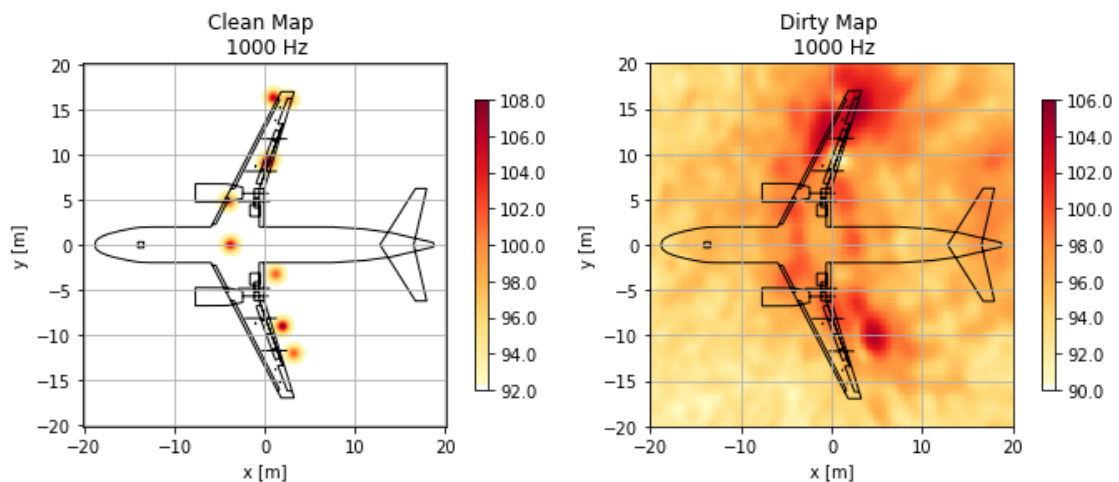


**Figure 4.36:** CLEAN results of an overflying measurement in 2016 at 1000 Hz with diagonal removal activated.

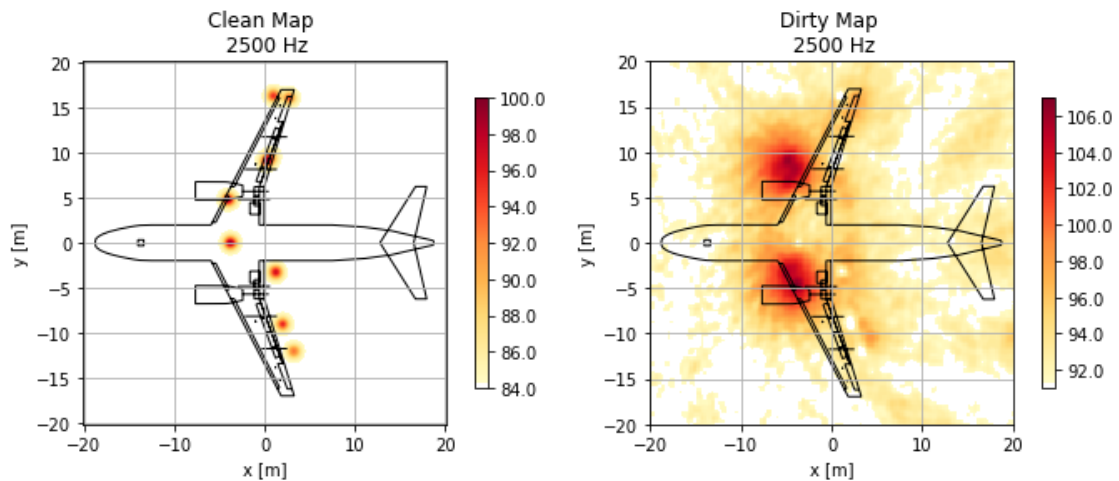


**Figure 4.37:** CLEAN results of an overflying measurement in 2016 at 2500 Hz with diagonal removal activated.

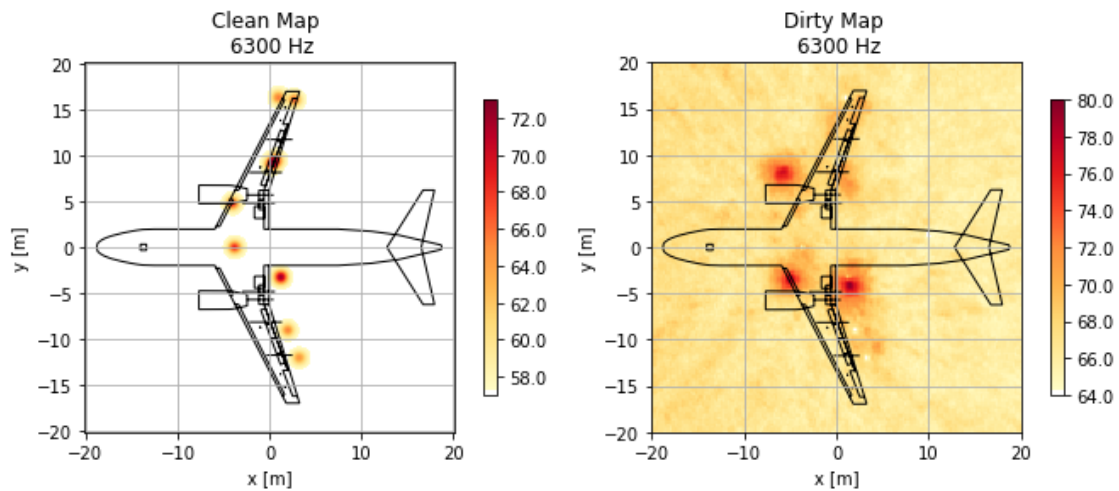


**Figure 4.38:** CLEAN results of an overflying measurement in 2016 at 6300 Hz with diagonal removal activated.

## 4.4 Recorded overflying measurements from 2019

A more tonal noise generated by the jet engines is present in this dataset which can be observed between 1000 – 2500 Hz in figure 4.39. This dataset is taken from a takeoff which means that the power output of the jet engines is at their maximum and thus the more tonal noise is present.

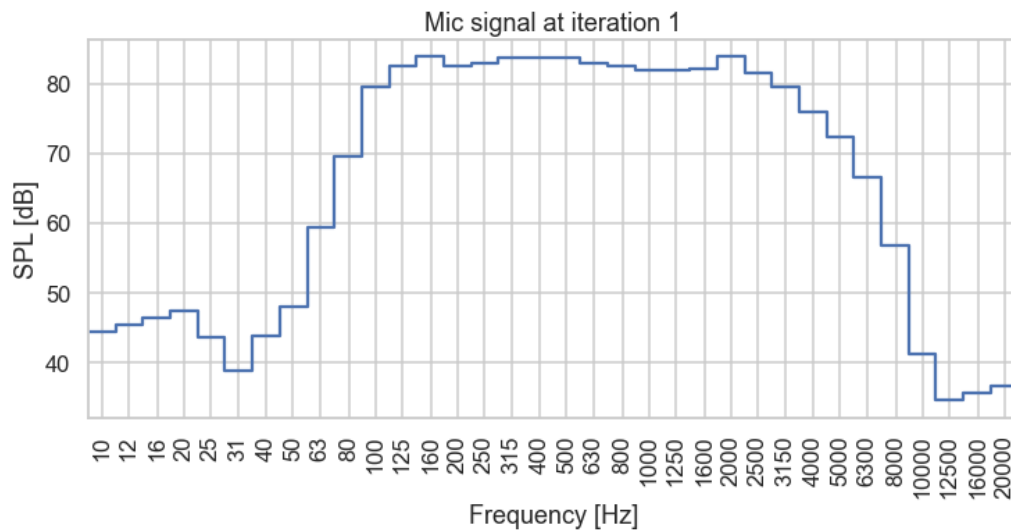


**Figure 4.39:** Recorded microphone signals in TOB only processed with the band-pass filter seen in figure 4.3.

#### 4.4.1 Diagonal removal deactivated

In this section the diagonal removal of the CSM is has been deactivated and a  $\gamma$  value of 0.6 is set.

These results reveal that the jet engines have been identified across all frequencies and again better detection for higher frequencies than lower. In this data the aircraft is taking of which means that the most dominant sound sources are from the jet engines. Sources are also identified in front of the engines which could be the BPF.

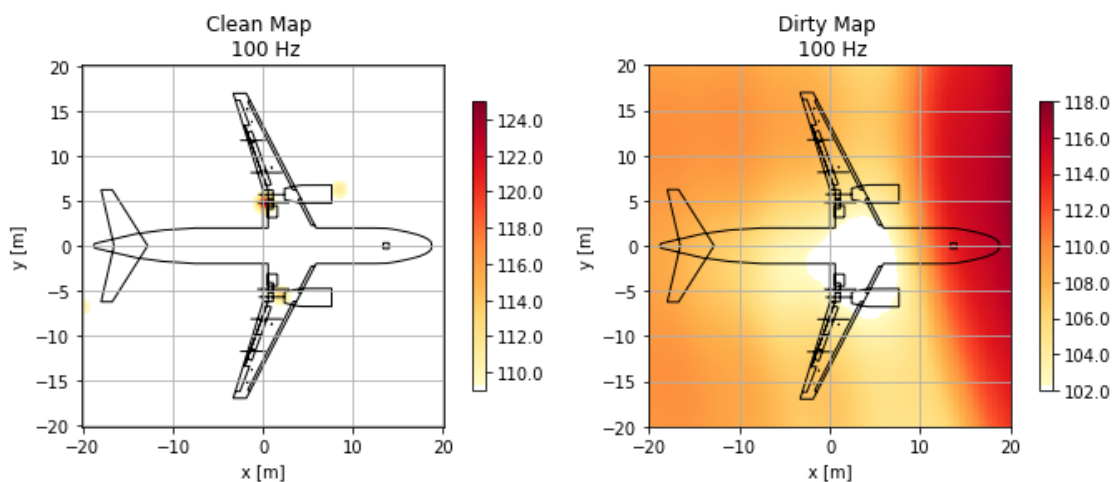


**Figure 4.40:** CLEAN results of an overflying measurement in 2019 at 100 Hz.

## 4. Results

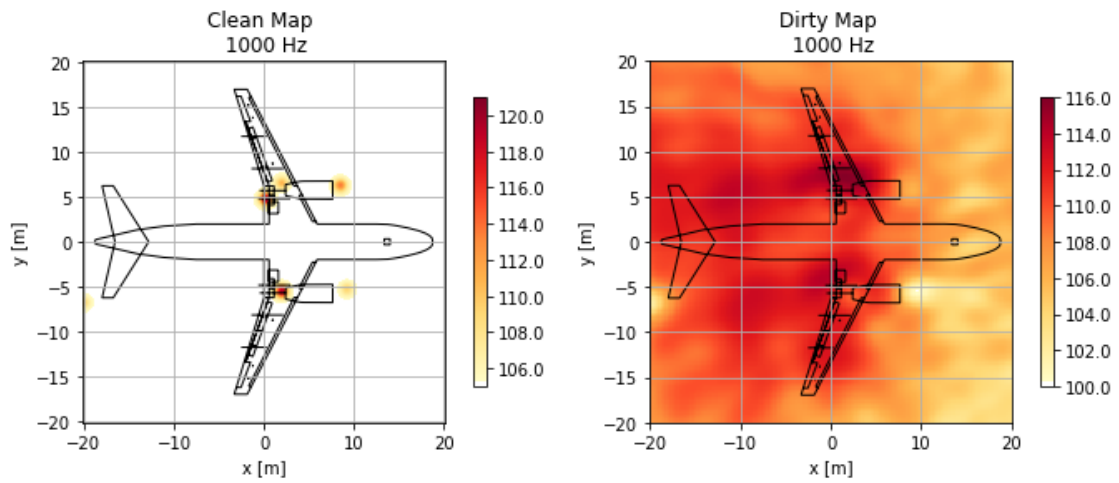


Figure 4.41: CLEANT results of an overflying measurement in 2019 at 1000 Hz.

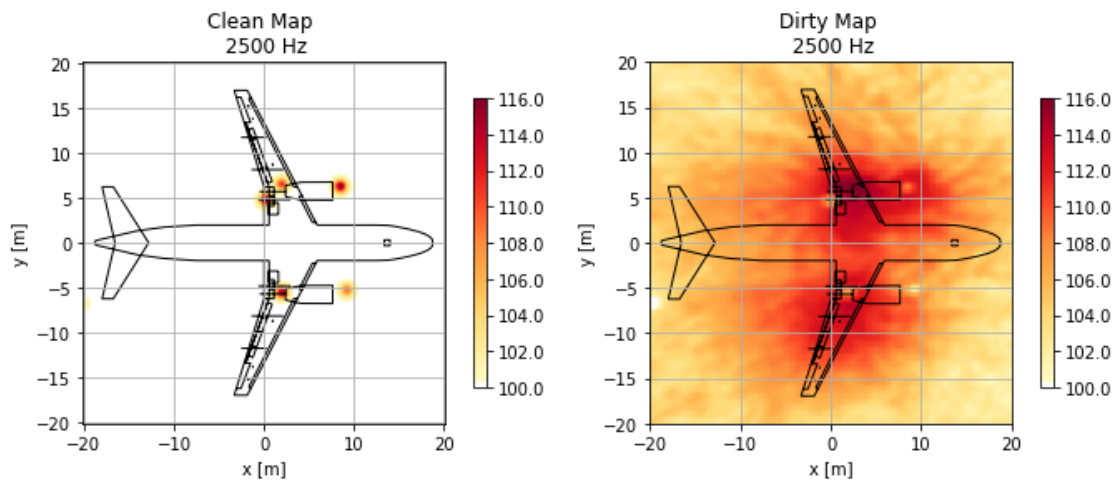


Figure 4.42: CLEANT results of an overflying measurement in 2019 at 2500 Hz.

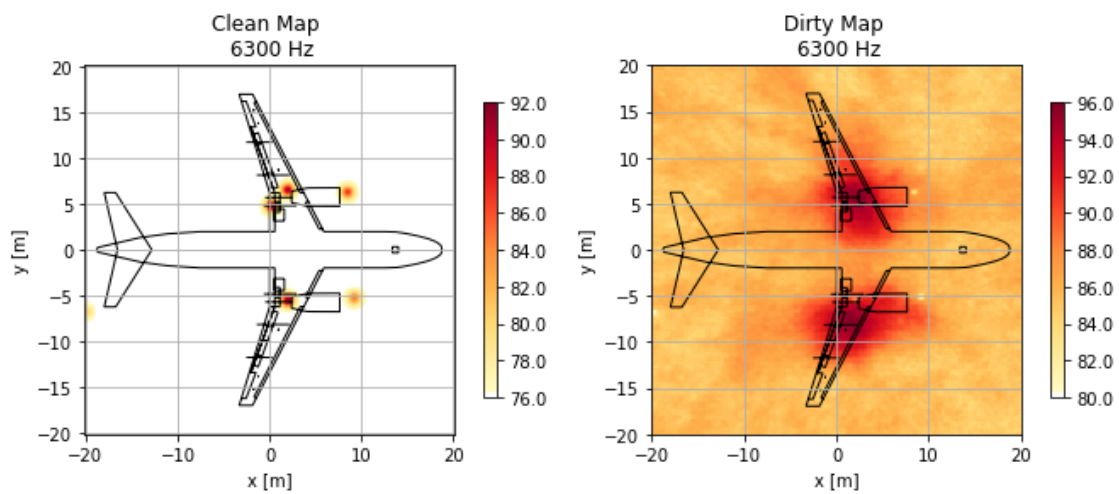
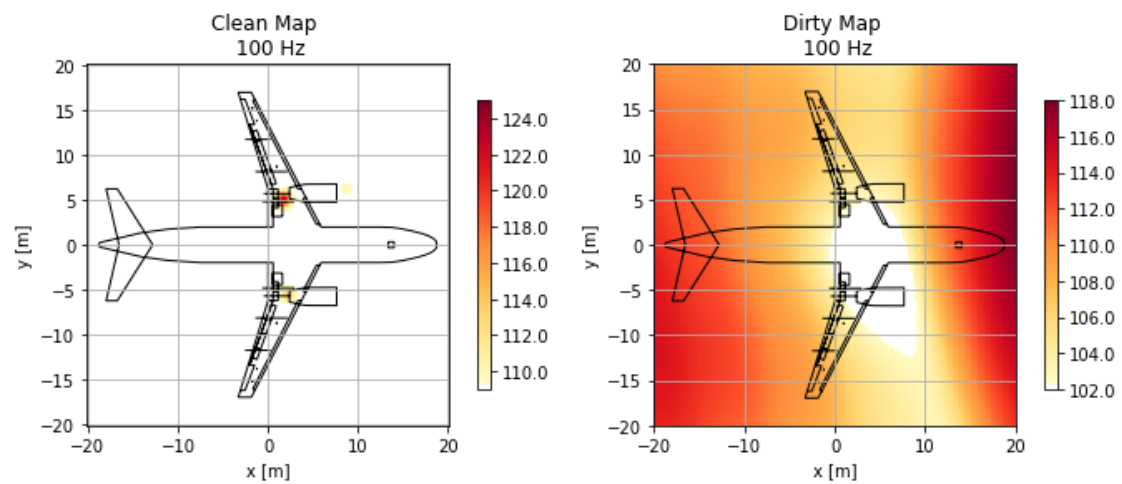


Figure 4.43: CLEANT results of an overflying measurement in 2019 at 6300 Hz.

### 4.4.2 Diagonal removal activated

In this section the diagonal removal of the CSM is active and a  $\gamma$  value of 0.6 is set.

When enabling diagonal removal the results generally looks better and the sound sources are higher in level. There are now more sound sources identified in front of the engines as well which are most like vortexes.



**Figure 4.44:** CLEANT results of an overflying measurement in 2019 at 100 Hz with diagonal removal activated.

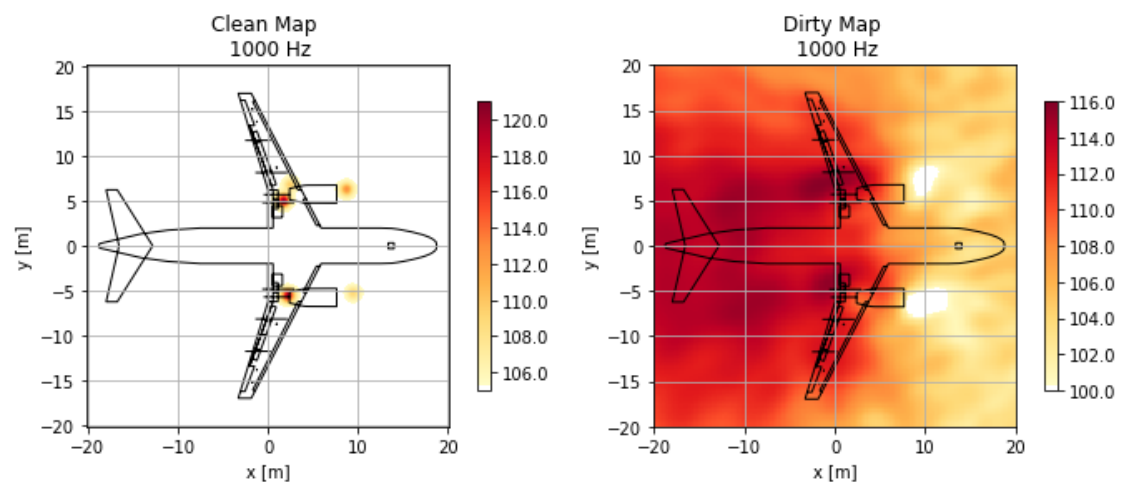


**Figure 4.45:** CLEANT results of an overflying measurement in 2019 at 1000 Hz with diagonal removal activated.

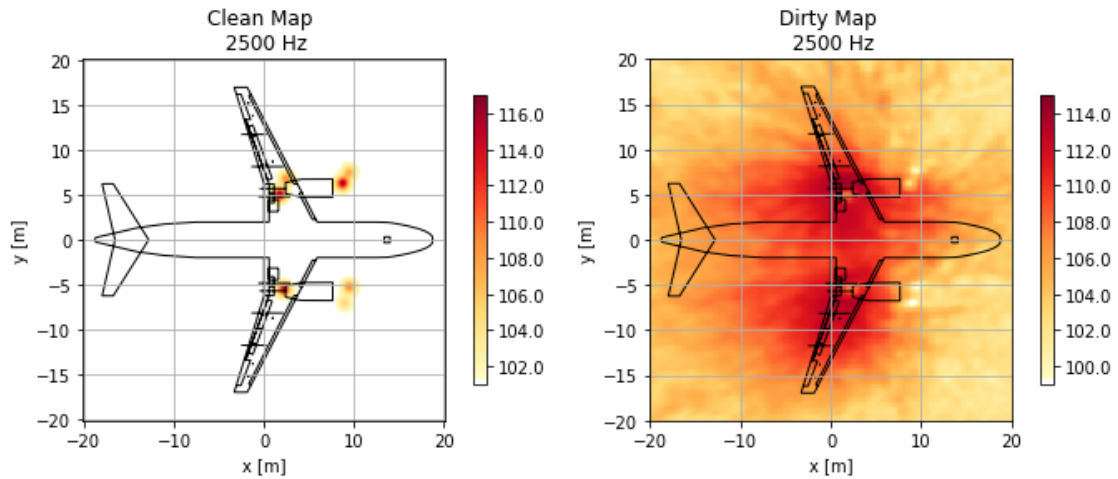


**Figure 4.46:** CLEAN results of an overflying measurement in 2019 at 2500 Hz with diagonal removal activated.

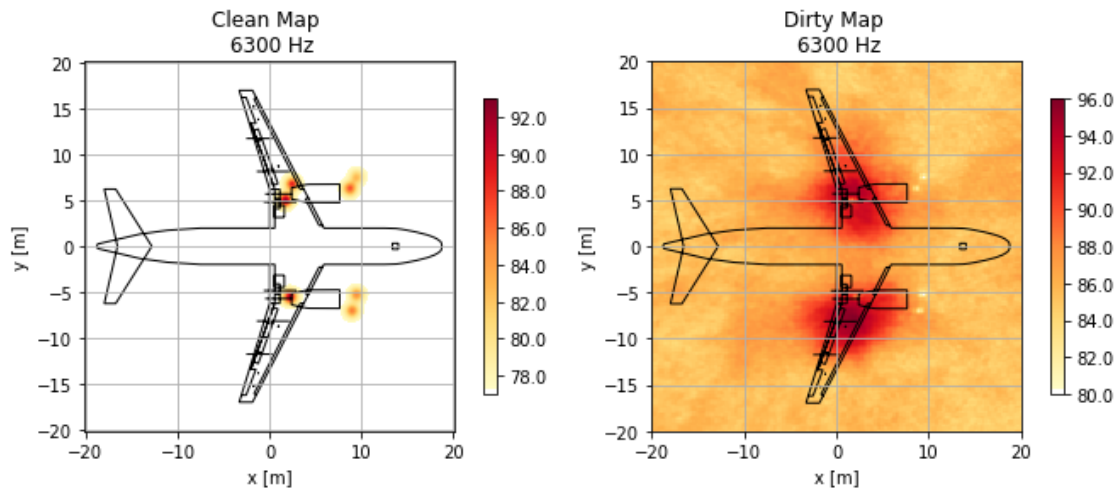


**Figure 4.47:** CLEAN results of an overflying measurement in 2019 at 6300 Hz with diagonal removal activated.

### 4.4.3 Diagonal removal activated and low loop gain

In this section the diagonal removal of the CSM is activated and a  $\gamma$  value of 0.1 is set.

Setting the gamma value to a very low one results in better detection and greater spread of the sound sources but with a significantly lower level. The individual sound sources are not easy to identify due to this spread but more sound sources have been located.

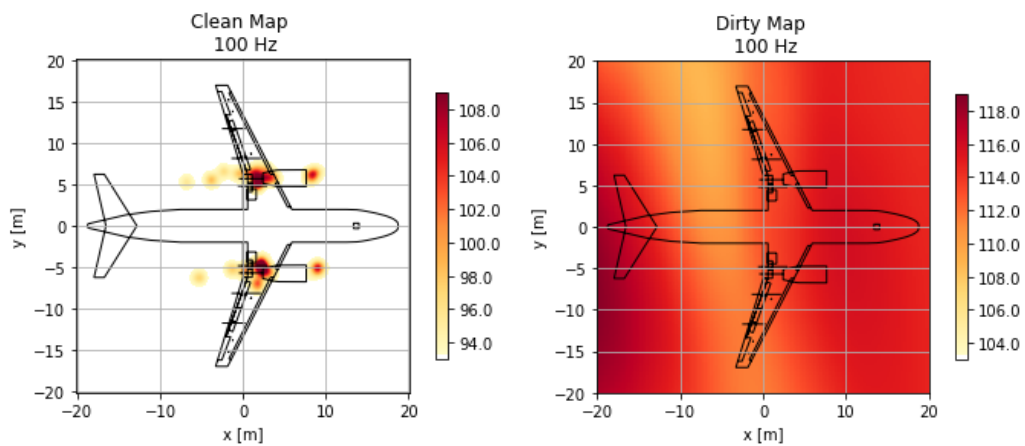


**Figure 4.48:** CLEANT results of an overflying measurement in 2019 at 100 Hz with diagonal removal activated and low gamma value.

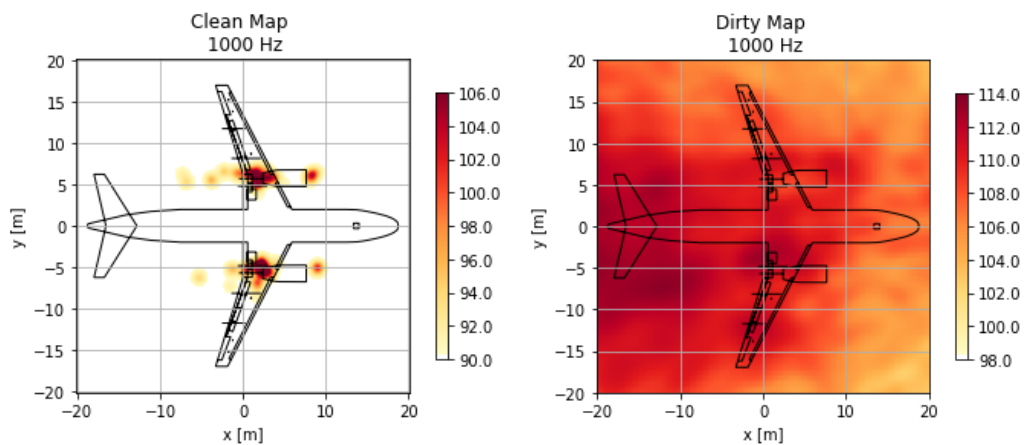


**Figure 4.49:** CLEANT results of an overflying measurement in 2019 at 1000 Hz with diagonal removal activated and low gamma value.

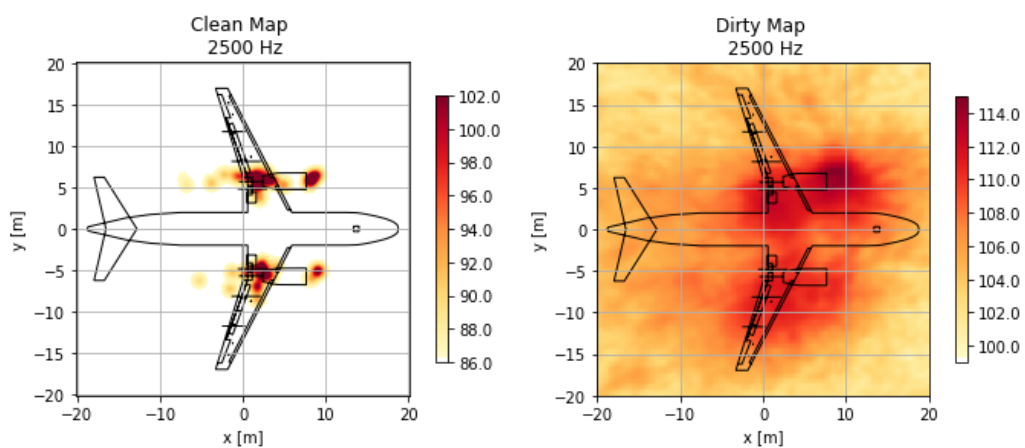


**Figure 4.50:** CLEANT results of an overflying measurement in 2019 at 2500 Hz with diagonal removal activated and low gamma value.

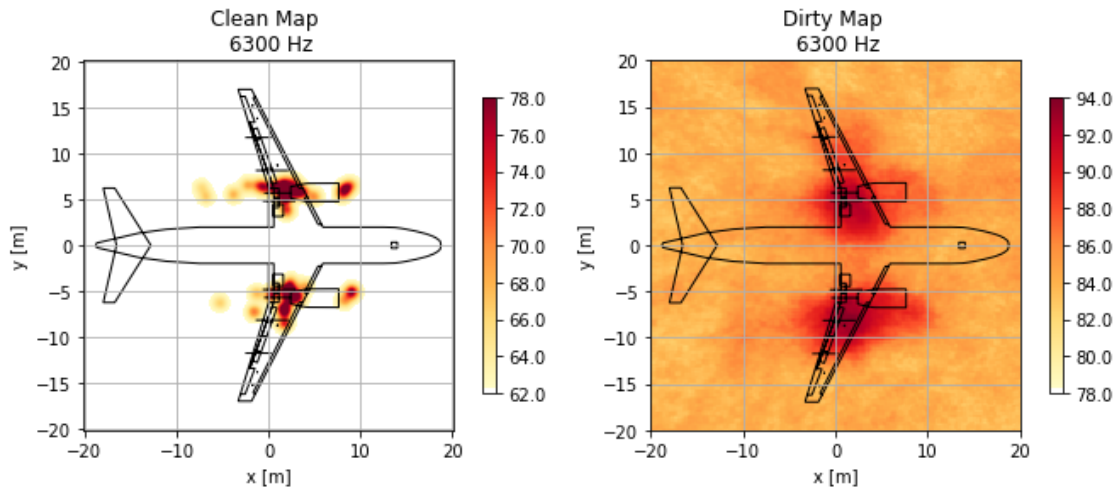


**Figure 4.51:** CLEAN results of an overflying measurement in 2019 at 6300 Hz with diagonal removal activated and low gamma value.

#### 4.4.4 Diagonal removal activated and single 1000 Hz TOB detection

In this section the diagonal removal of the CSM is activated and a  $\gamma$  value of 0.6 is set. The detection of the strongest source performed by the CLEAN algorithm is restricted to a single TOB of 1000 Hz.

Detection in a single TOB was quite useful for this data as the aircraft is taking meaning that the tonal components of the jet engines are more pronounced. The results reveals that more sources have been identified. Some sources from previous test cases have disappeared indicating that the new sources in this setup might be of more tonal characteristics.

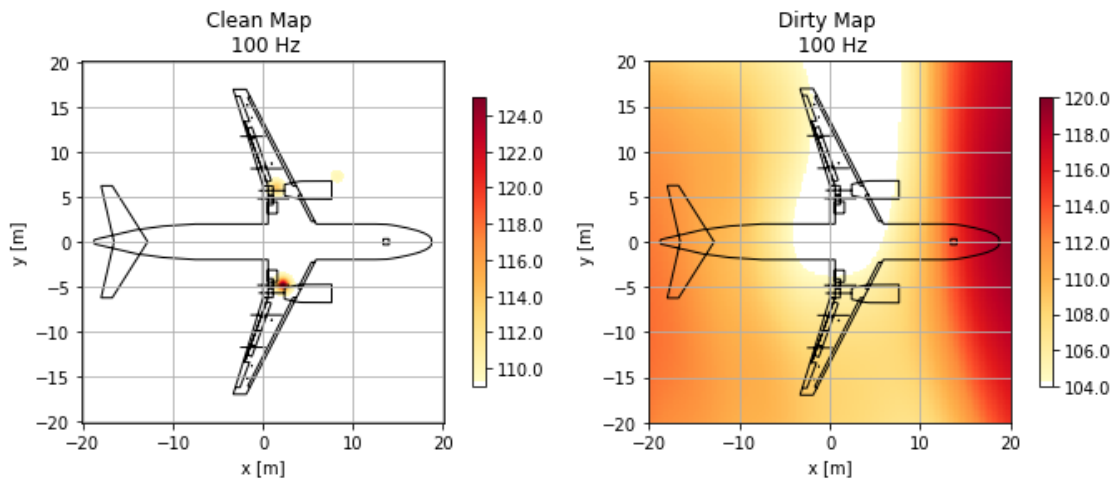


**Figure 4.52:** CLEAN results of an overflying measurement in 2019 at 100 Hz with diagonal removal activated and single TOB detection.

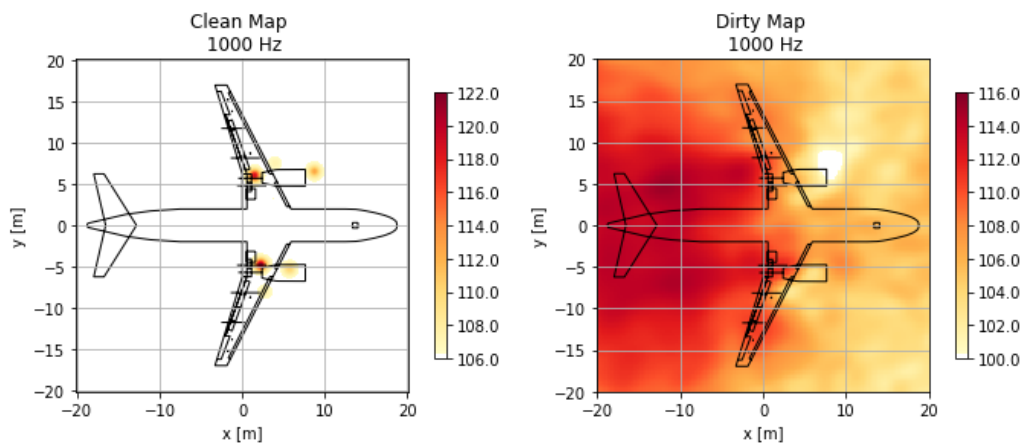


**Figure 4.53:** CLEANT results of an overflying measurement in 2019 at 1000 Hz with diagonal removal activated and single TOB detection.

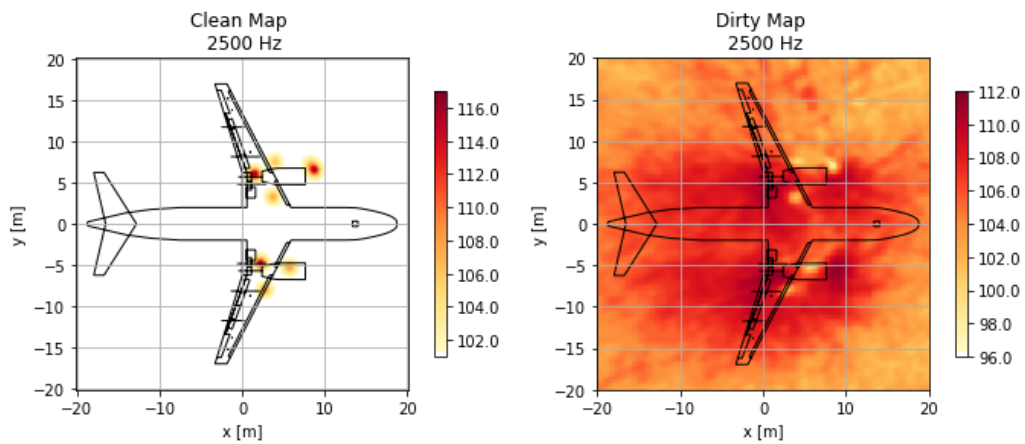


**Figure 4.54:** CLEANT results of an overflying measurement in 2019 at 2500 Hz with diagonal removal activated and single TOB detection.

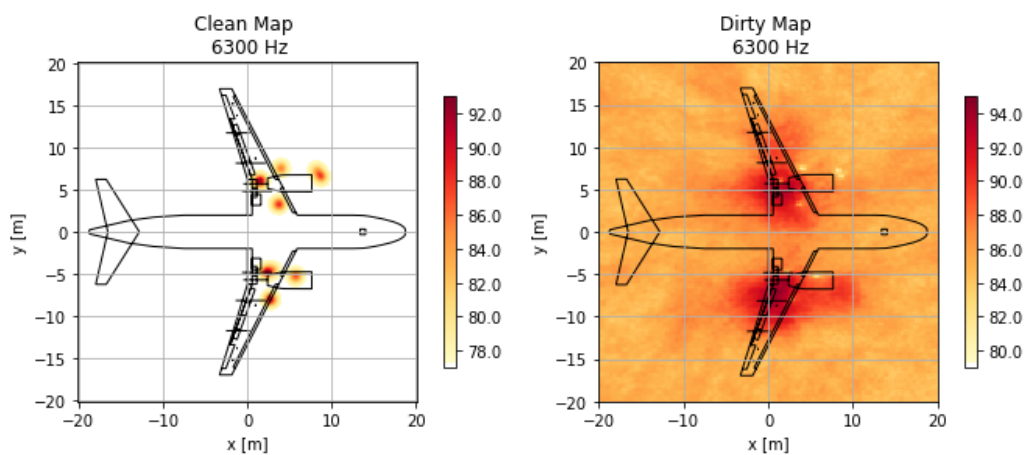


**Figure 4.55:** CLEANT results of an overflying measurement in 2019 at 6300 Hz with diagonal removal activated and single TOB detection.

#### 4.4.5 DAMAS vs. CLEANT

A comparison between DAMAS and CLEANT on the same dataset from 2019 where an airplane is taking off. For a fair comparison both algorithms used same grid size and settings, the only difference is that diagonal removal is active for CLEANT and not for DAMAS as it is not required unless a lot of noise is expected. Due to limitations of DAMAS at very low frequencies 100 Hz was replaced with 250 Hz.

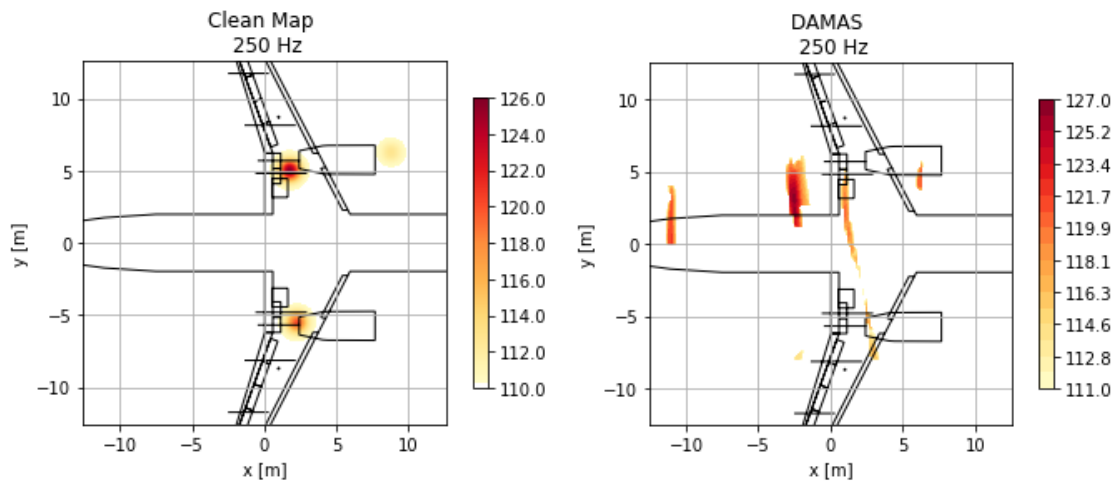


**Figure 4.56:** Results of an overflying measurement in 2019 (Left): CLEANT (Right): DAMAS, at 250 Hz.

The difference between CLEANT and DAMAS is significant for lower frequencies where CLEANT actually identifies sound sources whereas DAMAS mainly presents aliasing artifacts in figure 4.56.

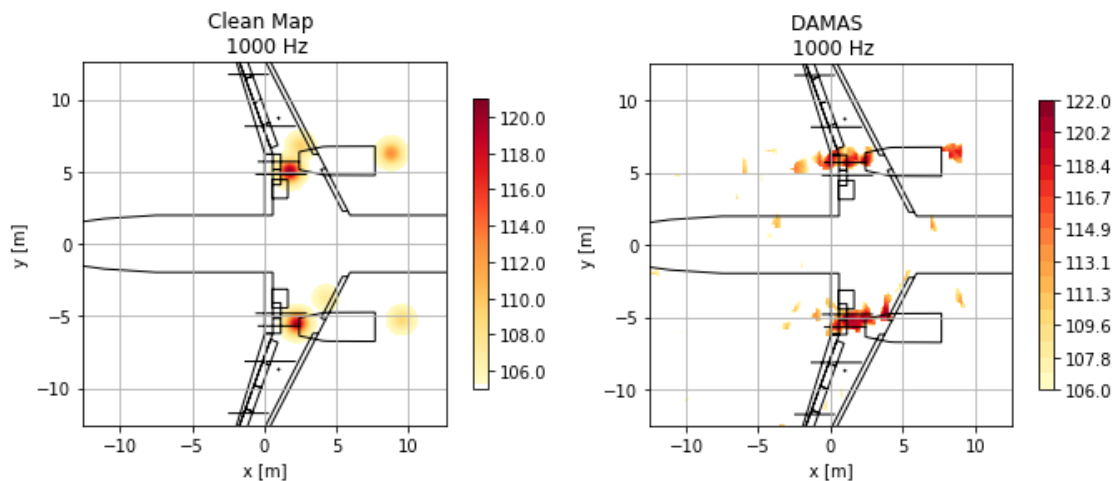


**Figure 4.57:** Results of an overflying measurement in 2019 (Left): CLEANT (Right): DAMAS, at 1000 Hz.

In the frequency range of 1000 Hz the identified sound sources are fairly similar. The DAMAS algorithm presents the identified sound sources in larger polygon shapes

while CLEANT on the other presents slightly better looking sources which makes it easier to separate the sound sources. There is a small difference in level as well between the two deconvolution algorithms which can be seen in figure 4.57.

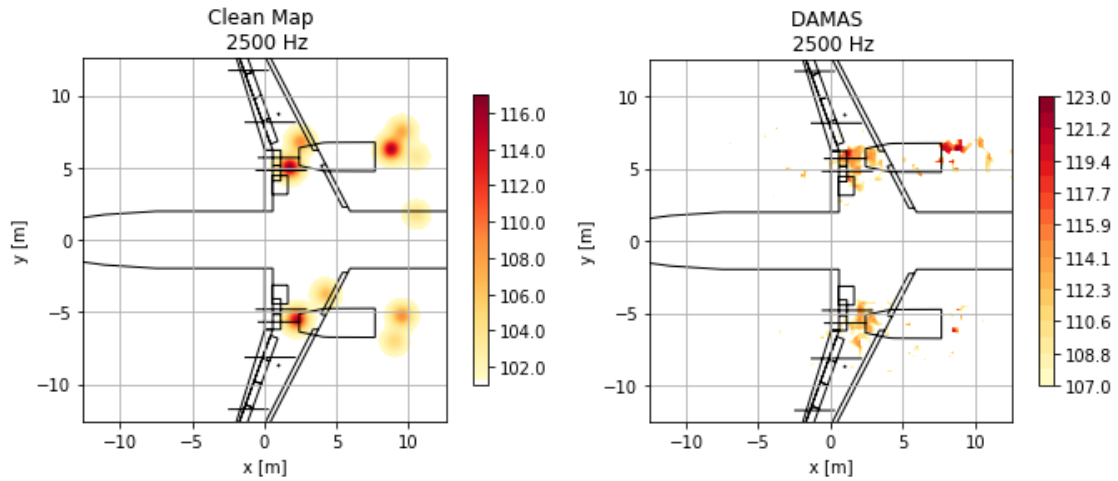


**Figure 4.58:** Results of an overflying measurement in 2019 (Left): CLEANT (Right): DAMAS, at 2500 Hz.

DAMAS is significantly improving its resolution with higher frequencies. in figure 4.58 there is a larger gap in level detection between CLEANT and DAMAS.

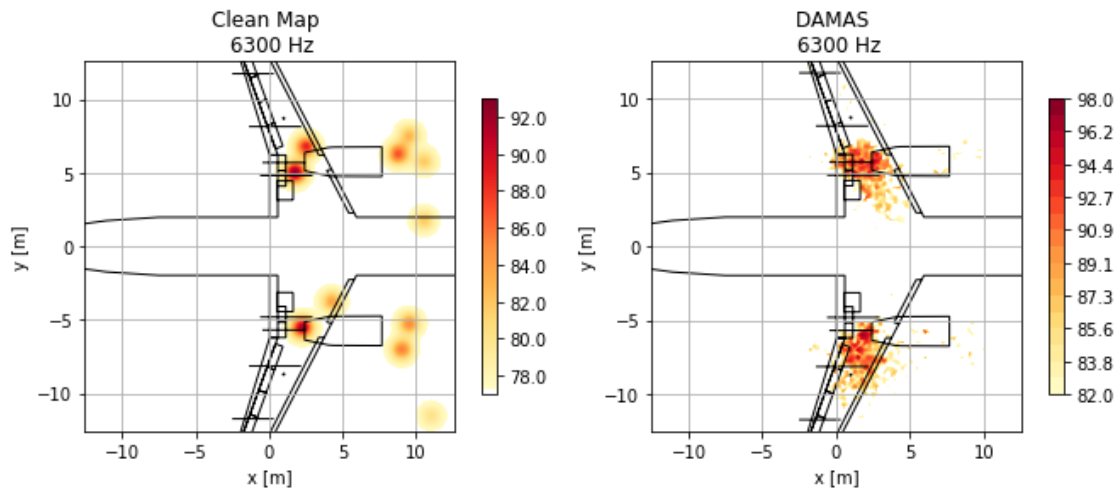


**Figure 4.59:** Results of an overflying measurement in 2019 (Left): CLEANT (Right): DAMAS, at 6300 Hz.

In figure 4.59 the resolution of DAMAS continues to improve but a lot of the sources in front of the engines are not longer detectable by DAMAS. CLEANT present even more identified sources in this frequency range both behind and in front of the jet engines. The sources behind the jet engines comes from the exhaust system. The sources in front are mainly vortexes and BPF.

# 5

## Analysis

The simulated datasets uses a grid of size  $41 \times 41$  where each step size is 0.25 m resulting in a grid covering  $10.25 \times 10.25$  m in total. For verification purposes of one or two sources this was considered enough as a greater grid size with smaller step size would heavily increase the computation cost. As long as the object which is being investigated, such as a simulated source or an aircraft, is covered by the entire grid there is no other purpose in increasing the grid size. In the first result section 4.1.1 CLEAN-T has processed a simulated overflying measurements of one sound source. For very low and very high frequencies there is a false sound source located to the left of the center positioned sound source. Although those are normal phenomena due to spatial undersampling of the microphone array, once diagonal removal is activated those false sources are gone. Diagonal removal provides an increased spatial accuracy in exchange for level accuracy, which can be observed in sections 4.1.1 and 4.1.2 for the figures representing the 1000 Hz sources. The same phenomenon can be observed in section 4.3.1 and where some sources disappear but the overall levels are lower when diagonal removal of the CSM is active. The sources detected in these figures are mainly caused by aerodynamic noise as the aircraft is approaching landing. A vortex can be observed at the tip of the right wing and the resistance caused by the extended wing flaps causes sources to be detected behind the wings.

In the section displaying the results of a simulated overflying measurements of two sound sources a greater variety of settings is tested such as different loop gain factor,  $\gamma$ , and localizing the strongest source within as single TOB. For the overflying measurements made in 2019 the same settings were investigated. In both these cases, section 4.2.3 and 4.4.3, the lower loop gain of  $\gamma = 0.1$  generates less accurate results. For the real overflying measurements from 2019 the lower loop gain causes a greater spread in sound source detection and thus making targeting of individual sources less accurate. In section 4.2.3 the lower loop gain results in the center positioned sound source to never be correctly detected in level although the source is identified except for at 100 Hz. Overall the levels are much lower with the lower loop gain compared to the other settings for the same case. This may not come as a surprise because that is what the loop gain controls, how much of a signal to add or remove. Unfortunately the algorithm is considered done when the energy within the dirty map increases from the previous iteration, meaning that what is left in the dirty map is considered the remaining noise. In section 4.2.4 and 4.4.4 the localization of the strongest source is restricted to a single TOB, in this case 1000 Hz TOB. Otherwise the detection of the strongest source is operating across the wide frequency band, 100 Hz to 10000 Hz. For the simulated data in section

4.2.4 only one source is detected at 100 Hz and for the higher frequencies the level of the right source is never fully detected. This may be that 1000 Hz TOB was a bad choice as the strongest signal may be in another frequency band. In section 4.4.4 the 1000 Hz TOB is more relevant as that is approximately the frequency range where the noise of jet engines are mainly located and the results are satisfying. The levels of the sources are slightly higher for this setting than when only diagonal removal is activated in section 4.4.2. Noise that is outside of this 1000 Hz TOB are unfortunately compromised for and are not properly detected, this can be seen at 6300 Hz in section 4.4.2 and 4.4.4. Although losing accuracy outside of the 1000 Hz TOB the accuracy is gained within the TOB. Generally diagonal removal seems to improve the results in all cases using CLEAN-T. The loop gain factor that yield the best results is  $\gamma = 0.6$  and it was achieved through trial and error.

In the very last section 4.4.5 the results from CLEAN-T are seen on the left side and DAMAS results are seen on the right side in different TOB. Beamforming settings were identical the only difference in these two cases is that diagonal removal is active for CLEAN-T and not for DAMAS. For 250 Hz TOB it is clearly visible that DAMAS has reached its limits and cannot detect the sources correctly, the spiral shapes indicates some sort of aliasing. The CLEAN-T on the other hand can detect sources and present them nicely. The strongest sources are detected at the exhaust system of the jet engines and the weaker source in front is most likely be the BPF of the jet engine. Overall the levels detected by DAMAS are higher than the ones detected by CLEAN-T where the difference is up to 7 dB for 2500 Hz. Source detection increases in resolution for higher frequencies using DAMAS where 250 Hz is not readable. At 1000 Hz the greatly resolution improves but the sources are still quite large and polygon shaped. For 2500 Hz and 6300 Hz DAMAS has excellent replication of the sources. This does not affect CLEAN-T as CLEAN-T does not suppress a PSF that is depending on the frequency.

# 6

## Conclusion

The goal of this study was to investigate and implement a more novel sound source localization algorithm in hopes of finding an approach which is more reliable, faster and extends the frequency band of operation. CLEANT is an algorithm that differs substantially from the previously used DAMAS by operating exclusively in the time domain. Both DAMAS and CLEANT have proven to be useful deconvolution approaches in pursuit of locating and quantifying sound sources of aircraft flyover measurements. CLEANT has shown that it can handle somewhat lower frequencies than DAMAS, where good results were achieved for as low as 100 Hz and due to its time domain property it allows for analysis across time and narrowband source spectrum. DAMAS on the other hand has a limit of operation around 200 Hz to 300 Hz. When it comes to accuracy the CLEANT algorithm has still not been verified to output correct SPL. This leaves room for future studies where the dedopplerized spectrum of the microphone signals can be compared to the output of the CLEANT results. For grid sizes up to around 25x25 m the two deconvolution algorithms operate at approximately the same speed where both approaches took between 4 – 5 hours to finish. With greater grid sizes of 40x40 m the CLEANT was finished in approximately 7 hours where DAMAS required approximately 32 hours. This means that the two algorithms scale very differently, CLEANT has a much more linear increase in computation cost than DAMAS. This might not come as a surprise because the heavy computation of CLEANT comes from performing beamforming for every iteration while DAMAS solves a large number of linear system equations of each frequency at almost every grid point. CLEANT of course has its limitations and depends on parameter settings such as loop gain factor. In some figures unexpected sources appear and some expected sources are missing due to its unique way of locating the strongest source in each iteration. This can be observed in figure 6.1 and 6.2. The variety of settings demonstrated in section 4 shows the sensitivity on user defined settings to obtain a better result. In all datasets the sources are identified and it is obvious that CLEANT can handle both broadband noises and tonal noises which is demonstrated in the overflying measurements from 2016 and 2019. In the results from 2016 CLEANT successfully locates the broadband noise generated by the extended wing flaps and vortexes which are dominant sources as the aircraft is approaching landing. In the results from overflying measurements from 2019 there is more emphasis on the jet engines noise, made up from broadband and tonal noise, as the aircraft is taking off.

Further research on CLEANT should investigate the possibilities of enhancing performance through more complex resampling and interpolation algorithms. In this

project resampling occurs before beamforming where the time data is sampled with 48 kHz and then resampled to 23.5 kHz. Resampling occurs once again when the modeled microphone signal is created from the strongest located source back to 48 kHz. Standard algorithms have been used due to the time frame of this project. This will increase the accuracy of the signal content for every iteration.

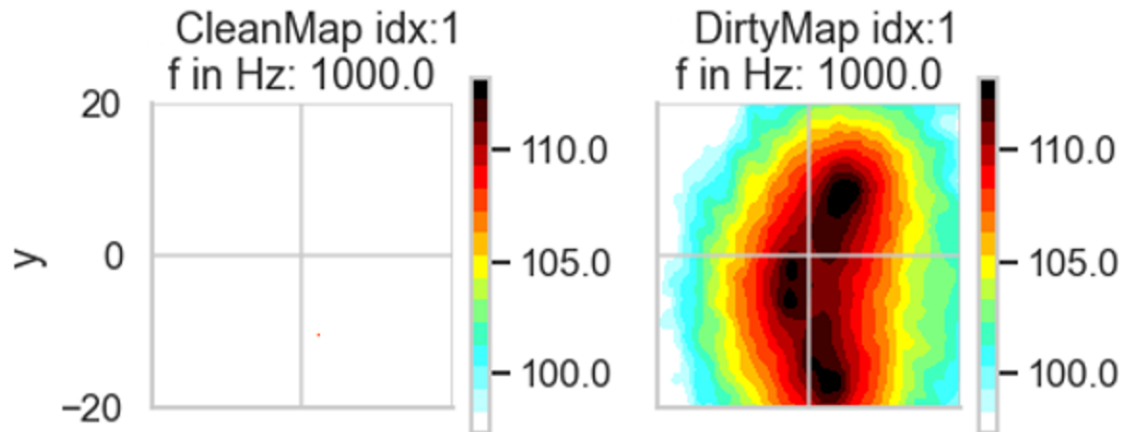


**Figure 6.1:** (Left): Clean Map at first iteration presenting the first located source. (Right): Dirty Map which is identical to the beamforming of the original microphone signal at first iteration.

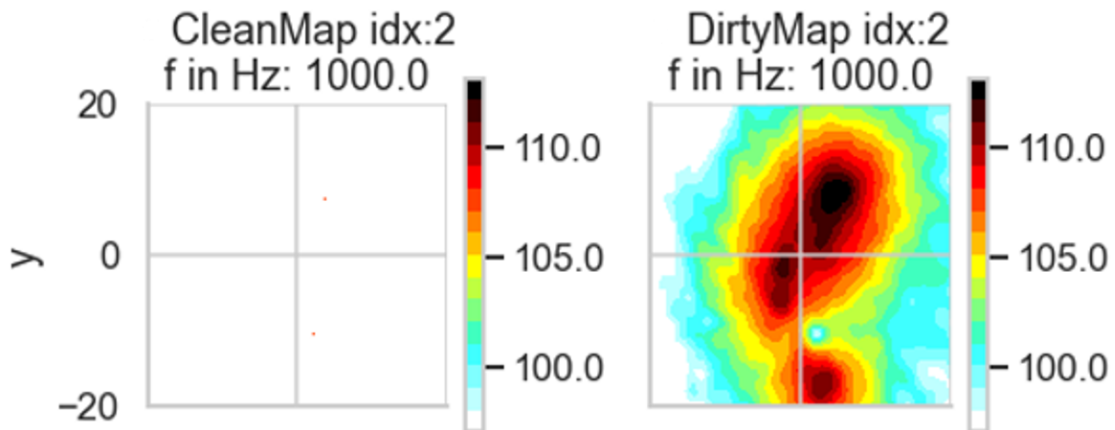


**Figure 6.2:** (Left): Clean Map at second iteration presenting two identified sources. (Right): Dirty Map now demonstrates the impact of the first identified strongest source being deleted from the Dirty Map.

# Bibliography

- [1] J. A. Högbom. “Aperture synthesis with a non-regular distribution of interferometer baselines”. In: *Astronomy and Astrophysics Supplement vol 15*. 1974.
- [2] A. Nordborg, J. Wedemann, and L. Willenbrink. “Optimum array microphone configuration”. In: *The 29th International Congress and Exhibition on Noise Control Engineering*. 2000.
- [3] Brooks and Humphreys. “A Deconvolution Approach for the Mapping of Acoustic Sources (DAMAS) Determined from Phased Microphone Arrays”. In: *10th AIAA/CEAS Aeroacoustics Conference, Manchester, Great Britain, May 10-12, 2004*. 2004.
- [4] U. Michel. “History of acoustic beamforming”. In: *1st Berlin Beamforming Conference*. 2006.
- [5] Sijtsma. “CLEAN Based on Spatial Source Coherence”. In: *13th AIAA/CEAS Aeroacoustics Conference, Rome, Italy, May 21-23, 2007*. 2007, AIAA-2007-3436.
- [6] Dougherty. “What is Beamforming?” In: *Proceedings on CD of the 2nd Berlin Beamforming Conference, 19-20 February, 2008*. GfAI, Gesellschaft zu Förderung angewandter Informatik e.V., Berlin, 2008. ISBN: 978-3-00-023849-9. URL: [http://bebec.eu/Downloads/BeBeC2008/Papers/BeBeC-2008-01\\_Dougherty.pdf](http://bebec.eu/Downloads/BeBeC2008/Papers/BeBeC-2008-01_Dougherty.pdf).
- [7] Guérin and Siller. “A Hybrid Time-Frequency Approach for the Source Localization Analysis of Acoustic Fly-over Tests”. In: *14th CEAS/AIAA Aeroacoustics Conference, Vancouver, British Columbia, Canada, 5-7 May 2008*. 2008.
- [8] Cousson et al. “Identification of Acoustic Moving Sources Using an Time-Domain Method”. In: *Proceedings on CD of the 7th Berlin Beamforming Conference, March 5-6, 2018*. GfAI, Gesellschaft zu Förderung angewandter Informatik e.V., Berlin, Mar. 2018. ISBN: 978-3-942709-20-0. URL: <http://www.bebec.eu/Downloads/BeBeC2018/Papers/BeBeC-2018-D17.pdf>.
- [9] T. Ellif, M. Cremaschi, and V. Huck. *Impact of aircraft noise pollution on residents of large cities*. 2020.
- [10] Kujawski and Sarradj. “Application of the CLEAN method for high speed railway train measurements”. In: *Proceedings on CD of the 8th Berlin Beamforming Conference, 2-3 March, 2020*. Mar. 2020. URL: <https://www.bebec.eu/fileadmin/bebec/downloads/bebec-2020/papers/BeBeC-2020-D02.pdf>.

- [11] R. Merino-Martínez et al. *A review of acoustic imaging methods using phased microphone arrays*. URL: <https://link.springer.com/content/pdf/10.1007/s13272-019-00383-4.pdf>. (accessed: 20.01.2022).
- [12] World Health Organization. *The burden of disease from environmental noise*. URL: [https://www.euro.who.int/\\_\\_data/assets/pdf\\_file/0008/136466/e94888.pdf](https://www.euro.who.int/__data/assets/pdf_file/0008/136466/e94888.pdf). (accessed: 19.01.2022).

DEPARTMENT OF SOME SUBJECT OR TECHNOLOGY  
CHALMERS UNIVERSITY OF TECHNOLOGY  
Gothenburg, Sweden  
[www.chalmers.se](http://www.chalmers.se)



**CHALMERS**  
UNIVERSITY OF TECHNOLOGY